

Parallel adaptive Bayesian quadrature for rare event estimation

Chao Dang^{a,*}, Pengfei Wei^b, Matthias G.R. Faes^c, Marcos A. Valdebenito^d, Michael Beer^{a,e,f}

^a*Institute for Risk and Reliability, Leibniz University Hannover, Callinstr. 34, Hannover 30167, Germany*

^b*School of Power and Energy, Northwestern Polytechnical University, Xi'an 710072, PR China*

^c*Chair for Reliability Engineering, TU Dortmund University, Leonhard-Euler-Str. 5, Dortmund 44227, Germany*

^d*Faculty of Engineering and Sciences, Universidad Adolfo Ibáñez, Av. Padre Hurtado 750, 2562340 Viña del Mar, Chile*

^e*Institute for Risk and Uncertainty, University of Liverpool, Liverpool L69 7ZF, United Kingdom*

^f*International Joint Research Center for Resilient Infrastructure & International Joint Research Center for Engineering Reliability and Stochastic Mechanics, Tongji University, Shanghai 200092, PR China*

Abstract

Various numerical methods have been extensively studied and used for reliability analysis over the past several decades. However, how to understand the effect of numerical uncertainty (i.e., numerical errors due to the discretization of the performance function) on the failure probability is still a challenging issue. The active learning probabilistic integration (ALPI) method offers a principled approach to quantify, propagate and reduce the numerical uncertainty via computation within a Bayesian framework, which has not been fully investigated in context of probabilistic reliability analysis. In this study, a novel method termed ‘Parallel Adaptive Bayesian Quadrature’ (PABQ) is proposed on the theoretical basis of ALPI, and is aimed at broadening its scope of application. First, the Monte Carlo method used in ALPI is replaced with an importance ball sampling technique **so as** to reduce the sample size that is needed for rare failure event estimation. Second, a **multi-point** selection criterion is proposed to enable parallel distributed processing. Four numerical examples are studied to demonstrate the effectiveness and efficiency of the proposed method. It is shown that PABQ can effectively assess small failure probabilities (e.g., as low as 10^{-7}) with a minimum number of iterations by taking advantage of parallel computing.

Keywords: Reliability analysis, Gaussian process, Numerical uncertainty, Bayesian quadrature, Parallel computing

1. Introduction

In many fields, reliability analysis has manifested itself as an essential tool to study the performance of a physical or an engineering system in the presence of uncertainties. A fundamental task in reliability analysis is to compute the probability of a predefined failure event, which is referred as failure probability. Let $\mathbf{X} = [X_1, X_2, \dots, X_d] \in \mathcal{X} \subseteq \mathbb{R}^d$ denote a vector of d random variables with known joint probability

*Corresponding author

31 density function (PDF) $f_{\mathbf{X}}(\mathbf{x})$. The performance function (also known as limit state function) is given as
 32 $y = g(\mathbf{x}) : \mathcal{X} \mapsto \mathcal{Y}$, by which the failure event $F = \{\mathbf{x} \in \mathcal{X} : g(\mathbf{x}) \leq 0\}$ is defined. The associated failure
 33 probability P_f is defined by the following multi-dimensional integral:

$$P_f = \int_{\mathcal{X}} I(\mathbf{x}) f_{\mathbf{X}}(\mathbf{x}) d\mathbf{x}, \quad (1)$$

34 where $I(\mathbf{x})$ is the failure indicator function, which is defined as:

$$I(\mathbf{x}) = \begin{cases} 1, & \text{if } g(\mathbf{x}) \leq 0 \\ 0, & \text{otherwise} \end{cases}. \quad (2)$$

35 To assess the failure probability defined in Eq. (1), a variety of numerical methods have been extensively
 36 studied and applied by researchers and engineers over the past several decades. In general, the existing
 37 methods can be roughly classified into five categories:

- 38 1. Stochastic simulation methods, e.g., Monte Carlo simulation (MCS) and its variants (e.g., Subset
 39 Simulation (SS) [1] and Importance Sampling (IS) [2, 3]). Despite of their relative robustness to the
 40 dimension and complexity of the problem at hand, most of the stochastic simulation methods involve a
 41 considerable number of deterministic simulations, and hence are still very computationally demanding,
 42 especially for an expensive computational model with a small failure probability;
- 43 2. Asymptotic approximation methods, such as first-order reliability method (FORM) [4, 5] and second-
 44 order reliability method (SORM) [6, 7]. This kind of methods relies on the first- or second-order
 45 Taylor expansion of the limit state surface at the most probable point (MPP). Hence, its application
 46 is challenging whenever one must deal with multiple MPPs and highly nonlinear problems. Besides,
 47 FORM and SORM only yield approximate results in general cases, and provide no measure of the
 48 error introduced by the expansion;
- 49 3. Moment methods, for instance, integer moment based methods [8, 9, 10], fractional moment based
 50 methods [11, 12, 13], moment-generating function (or Laplace transform) based methods [14, 15, 16].
 51 The basic idea of these methods is to fit a proper probability distribution to the output variable
 52 of a performance function based on the knowledge of its estimated moments of certain type, which,
 53 however, typically leads to an ill-posed inverse problem (i.e., the so-called classical moment problem).
 54 Moreover, the estimation errors arising from both the estimated moments and assumed probability
 55 distribution model could be intractable to assess and handle;
- 56 4. Probability-conservation based methods, including, e.g., probability density evolution method [17,
 57 18, 19, 20] and direct probability integral method [21, 22, 23, 24]. These methods are established on
 58 rigorous theoretical fundamentals, but may still suffer from numerical difficulty especially for problems
 59 with high-dimensional inputs and/or rare failure events;

5. Surrogate assisted methods. This type of methods is of special interest in the present paper since the proposed method also falls in this category in some sense.

Surrogate assisted methods aim at constructing an inexpensive-to-evaluate surrogate model in place of the original expensive-to-evaluate performance function based on a limited number of its observations. Then, for example, stochastic simulation methods can be directly applied in conjunction with the surrogate model to produce a failure probability estimate. Typical surrogate models for reliability analysis include response surface methods [25, 26, 27], support vector machines [28, 29, 30], polynomial chaos expansions [31, 32], Gaussian process regression (GPR, also known as Kriging) [33, 34, 35], etc. In addition to developing new surrogate models, there has been growing attention paid to adaptive (optimal) design of experiments for training these surrogates. In this line, the GPR model is of particular interest for constructing an adaptive meta-model due to its attractive features, especially for active learning sampling strategies. Representative learning functions consist of the expected feasibility [36], U [37], expected risk [38], H [39], least improvement [40], reliability-based expected improvement [41], folded normal based expected improvement [42], upper-bound posterior variance contribution (UPVC) [43] and so forth. Besides, the following three aspects have also been paid special attention to in recent publications:

1. assessing small failure probabilities. In addition to MCS, other stochastic simulation methods requiring less samples are combined with active learning Kriging (AK) to evaluate small failure probabilities. Representative works include, e.g., AK-IS [44], meta-IS [34], AK-SS [45] and AK-MCMC (Markov chain Monte Carlo) [46], etc;
2. addressing high-dimensional problems. This aspect is mainly tackled by using some dimension-reduction techniques, e.g., active subspace methods [47, 48], principal component analysis [49, 50, 51], sufficient dimension reduction [52] and sliced inverse regression [53], etc;
3. enabling parallel computing. Most existing learning functions can only identify one point at each iteration, hindering the use of ever-increasing parallel-computing facilities. To overcome this obstacle, tailored strategies have been proposed, which are mainly based on applying clustering algorithms, such as k -means clustering [34], density clustering [54], spectral clustering [55] and k -medoids clustering [56].

The interested reader can refer to [57] for a comprehensive review. Despite great efforts, most existing Kriging assisted methods still possess respective limitations, and leave room for further improvement in terms of applicability, efficiency and accuracy.

In fact, Gaussian process model can be used in a different way, instead of a pure surrogate model. The first author and his co-workers proposed an active learning probabilistic integration (ALPI) method in a recent paper [43]. In this method, a Bayesian perspective is advocated to reinterpret failure probability integral estimation. By placing a prior distribution (i.e., Gaussian process) over the performance function, we finally arrive at a posterior distribution over the failure probability conditional on some observations of

94 the performance function. The **induced** posterior distribution of the failure probability reflects the fact that
95 the performance function has been discretised, **and hence numerical uncertainty arises due to discretization**
96 **error**. A novel feature of ALPI is that the numerical uncertainty can be properly quantified, propagated and
97 reduced via computation, which distinguishes it from other existing methods. Unfortunately, the idea is only
98 investigated in the context of imprecise probabilities, and lacks of comprehensive studies for probabilistic
99 reliability analysis.

100 In this paper, the ALPI method is specially studied under the framework of precise probabilities. The
101 basic idea is explained in a detailed way, and some limitations existing in the previous numerical algorithm
102 are identified. Most importantly, we propose a new method called ‘Parallel Adaptive Bayesian Quadra-
103 ture’ (PABQ) on the theoretical basis of the original ALPI method, while alleviating its main limitations.
104 Compared to ALPI, PABQ has two significant advantages. First, PABQ can select multiple points at each
105 iteration, and as such supports parallel distributed processing. Second, PABQ can assess very small fail-
106 ure probabilities without generating a prohibitively large number of candidate samples. Additionally, the
107 Matlab code of the developed method is freely available to the public ¹.

108 The outline of the remaining paper is as follows. The original ALPI method is revisited in Section 2
109 and the theoretical foundations are deepened. Section 3 gives the newly developed PABQ method. Four
110 numerical examples are investigated in Section 4 to illustrate the performance of the PABQ method. Section
111 5 gives some concluding remarks of the present study.

112 2. Active learning probabilistic integration

113 This section gives a review of the ALPI method. In comparison to [43], we will explain the basic idea
114 of ALPI in a more detailed and rigorous way, and provide its numerical algorithm that was omitted in [43].
115 Besides, the advantages and disadvantages of the method will be discussed.

116 2.1. Theoretical background

117 The ALPI method offers a Bayesian approach to approximating the intractable failure probability inte-
118 gral, which is defined in Eq. (1). The method is strongly motivated by Bayesian (probabilistic) integration
119 (also well known as Bayesian quadrature or cubature) [58, 59, 60]. To be specific, the ALPI method turns
120 the task of failure probability estimation into a Bayesian inference problem from limited data, as opposed to
121 classical frequentist inference. To do so, we think of the g -function as being random. This is understandable
122 in the Bayesian sense that the numerical value of $g(\mathbf{x})$ is always unknown until we actually evaluate $g(\cdot)$
123 at some point \mathbf{x} , though the g -function is said to be deterministic. Such interpretation is justified since
124 we can not afford to compute $g(\cdot)$ at every possible location. In this regard, epistemic uncertainty due to

¹to be released upon acceptance of the paper

125 discretisation error arises where the g -function is not evaluated. This kind of uncertainty will propagate into
 126 the failure indicator function $I(\mathbf{x})$ and will therefore affect the failure probability estimate. Consequently,
 127 the epistemic uncertainty should be properly treated within our computational framework, because it is
 128 not always negligible, especially when the available observations are scarce. Following a standard Bayesian
 129 approach, the ALPI method is intended to quantify, propagate and reduce the epistemic uncertainty. Specif-
 130 ically, ALPI first assigns a prior distribution over the g -function. Then, conditioning on some observations
 131 $\mathcal{D} = \{\mathcal{X}, \mathcal{Y}\}$ ($\mathcal{X} = \{\mathbf{x}^{(i)}\}_{i=1}^n$ with $\mathbf{x}^{(i)}$ being the i -th row of \mathcal{X} and $\mathcal{Y} = \{y^{(i)}\}_{i=1}^n$ with $y^{(i)} = g(\mathbf{x}^{(i)})$ being
 132 the i -th row of \mathcal{Y}), gives arise to a posterior distribution of g according to Bayes' rule. This will in turn
 133 imply a posterior distribution over $I(\mathbf{x})$, and so does over P_f . Technical details of ALPI will be discussed
 134 below.

135 ALPI starts by placing a Gaussian process (GP) prior over the g -function, which is written as:

$$\hat{g}_0 \sim \mathcal{GP}(m_{\hat{g}_0}(\mathbf{x}), k_{\hat{g}_0}(\mathbf{x}, \mathbf{x}')), \quad (3)$$

136 where \hat{g}_0 denotes the prior distribution of g before seeing any observations; $m_{\hat{g}_0}(\mathbf{x})$ and $k_{\hat{g}_0}(\mathbf{x}, \mathbf{x}')$ are the
 137 prior mean and covariance functions respectively, by which the GP model can be completely characterized.
 138 Among many options for $m_{\hat{g}_0}(\mathbf{x})$ and $k_{\hat{g}_0}(\mathbf{x}, \mathbf{x}')$ in the literature, without loss of generality the constant
 139 prior mean is adopted (i.e., $m_{\hat{g}_0}(\mathbf{x}) = \beta$), and the prior covariance function takes the squared exponential
 140 kernel:

$$k_{\hat{g}_0}(\mathbf{x}, \mathbf{x}') = \sigma^2 \exp\left(-\frac{1}{2}(\mathbf{x} - \mathbf{x}')^\top \boldsymbol{\Sigma}^{-1}(\mathbf{x} - \mathbf{x}')\right), \quad (4)$$

141 where σ^2 with $\sigma > 0$ denotes the process variance; $\boldsymbol{\Sigma} = \text{diag}(l_1^2, l_2^2, \dots, l_d^2)$ with $l_i > 0$ being the length scale
 142 in the i -th dimension, and $\text{diag}(\cdot)$ forms a diagonal matrix whose diagonal elements are its arguments. The
 143 $d + 2$ parameters collected in $\boldsymbol{\vartheta} = \{\beta, \sigma, l_1, l_2, \dots, l_d\}$ are referred to hyper-parameters to be determined. In
 144 a fully Bayesian fashion, those hyper-parameters should also be specified by Bayesian inference (see, e.g.,
 145 [61]). However, this will render the posterior distribution of g analytically intractable. For this reason, it
 146 was not explored in ALPI.

147 Alternatively, given the data \mathcal{D} , the hyper-parameters are fitted by minimizing the negative log marginal
 148 likelihood (NLML) $\mathcal{L}(\boldsymbol{\vartheta})$:

$$\hat{\boldsymbol{\vartheta}} = \arg \min_{\boldsymbol{\vartheta}} \mathcal{L}(\boldsymbol{\vartheta}), \quad (5)$$

149 with the NLML $\mathcal{L}(\boldsymbol{\vartheta})$ being:

$$\mathcal{L}(\boldsymbol{\vartheta}) = -\log [p(\mathcal{Y}|\mathcal{X}, \boldsymbol{\vartheta})] = \frac{1}{2}(\mathcal{Y} - \beta)^\top \mathbf{K}_{\hat{g}_0}^{-1}(\mathcal{Y} - \beta) + \frac{1}{2} \log [|\mathbf{K}_{\hat{g}_0}|] + \frac{n}{2} \log [2\pi], \quad (6)$$

150 where $p(\mathcal{Y}|\mathcal{X}, \boldsymbol{\vartheta})$ is the marginal likelihood following a normal distribution; $\mathbf{K}_{\hat{g}_0}$ is the covariance matrix
 151 with (i, j) -th entry $[\mathbf{K}_{\hat{g}_0}]_{i,j} = k_{\hat{g}_0}(\mathbf{x}^{(i)}, \mathbf{x}^{(j)})$.

152 Once the point estimate hyper-parameters $\hat{\boldsymbol{\vartheta}}$ are obtained, it turns out that the posterior distribution of
 153 g can be derived in closed form, i.e., another GP:

$$\hat{g}_n \sim \mathcal{GP}(m_{\hat{g}_n}(\mathbf{x}), k_{\hat{g}_n}(\mathbf{x}, \mathbf{x}')), \quad (7)$$

154 where \hat{g}_n denotes the posterior distribution of g conditional on \mathcal{D} ; $m_{\hat{g}_n}(\mathbf{x})$ and $k_{\hat{g}_n}(\mathbf{x}, \mathbf{x}')$ are the posterior
 155 mean and covariance functions respectively, which are analytically available:

$$m_{\hat{g}_n}(\mathbf{x}) = m_{\hat{g}_0}(\mathbf{x}) + \mathbf{k}_{\hat{g}_0}(\mathbf{x}, \mathcal{X})^\top \mathbf{K}_{\hat{g}_0}^{-1}(\mathcal{Y} - \mathbf{m}_{\hat{g}_0}(\mathcal{X})), \quad (8)$$

$$k_{\hat{g}_n}(\mathbf{x}, \mathbf{x}') = k_{\hat{g}_0}(\mathbf{x}, \mathbf{x}') - \mathbf{k}_{\hat{g}_0}(\mathbf{x}, \mathcal{X})^\top \mathbf{K}_{\hat{g}_0}^{-1} \mathbf{k}_{\hat{g}_0}(\mathbf{x}', \mathcal{X}), \quad (9)$$

157 where $\mathbf{m}_{\hat{g}_0}(\mathcal{X})$ is an $n \times 1$ mean vector with i -th element being $m_{\hat{g}_0}(\mathbf{x}^{(i)})$; $\mathbf{k}_{\hat{g}_0}(\mathbf{x}, \mathcal{X})$ is an $n \times 1$ covariance
 158 vector with i -th entry being $k_{\hat{g}_0}(\mathbf{x}, \mathbf{x}^{(i)})$; $\mathbf{k}_{\hat{g}_0}(\mathbf{x}', \mathcal{X})$ is defined in a way similar to $\mathbf{k}_{\hat{g}_0}(\mathbf{x}, \mathcal{X})$. Note that in
 159 Eqs. (8) and (9) $\boldsymbol{\vartheta}$ should be updated with $\hat{\boldsymbol{\vartheta}}$.

160 It can be deduced that the posterior distribution of failure indicator function I follows a generalized
 161 Bernoulli process ² (GBP):

$$\hat{I}_n \sim \mathcal{GBP}(m_{\hat{I}_n}(\mathbf{x}), k_{\hat{I}_n}(\mathbf{x}, \mathbf{x}')), \quad (10)$$

162 where \hat{I}_n denotes the posterior distribution of I conditional on \mathcal{D} ; $m_{\hat{I}_n}(\mathbf{x})$ and $k_{\hat{I}_n}(\mathbf{x}, \mathbf{x}')$ are the posterior
 163 mean and covariance functions respectively. The posterior mean of I can be derived in closed form [43]:

$$m_{\hat{I}_n}(\mathbf{x}) = \Phi\left(-\frac{m_{\hat{g}_n}(\mathbf{x})}{\sigma_{\hat{g}_n}(\mathbf{x})}\right), \quad (11)$$

164 where Φ is the cumulative distribution function of the standard normal distribution; $\sigma_{\hat{g}_n}(\mathbf{x})$ is the posterior
 165 standard derivation (STD) function of g , i.e., $\sigma_{\hat{g}_n}(\mathbf{x}) = \sqrt{k_{\hat{g}_n}(\mathbf{x}, \mathbf{x})}$. The posterior covariance function of I ,
 166 however, is not analytically tractable. Only closed-form expression for its posterior variance function $\sigma_{\hat{I}_n}^2(\mathbf{x})$
 167 is available [43]:

$$\sigma_{\hat{I}_n}^2(\mathbf{x}) = \Phi\left(-\frac{m_{\hat{g}_n}(\mathbf{x})}{\sigma_{\hat{g}_n}(\mathbf{x})}\right) \Phi\left(\frac{m_{\hat{g}_n}(\mathbf{x})}{\sigma_{\hat{g}_n}(\mathbf{x})}\right). \quad (12)$$

168 The posterior distribution $\hat{P}_{f,n}$ of failure probability P_f conditional on the data \mathcal{D} should thus follow
 169 a random variable, which reflects our epistemic uncertainty about P_f , due to the limited number of obser-
 170 vations. Note that the exact posterior distribution of P_f , however, is not known. Instead, the posterior
 171 mean and variance of P_f should be more of interest, where the posterior mean corresponds to the failure
 172 probability predictor and the posterior variance measures the prediction uncertainty. By applying Fubini's

²'generalized' indicates that the Bernoulli process considered here is location-dependent, in contrast to not considering the dependence in conventional definition of a Bernoulli process.

173 theorem, the posterior mean and variance of P_f can be derived as [43]:

$$\begin{aligned}
m_{\hat{P}_{f,n}} &= \mathbb{E}_{\hat{I}_n} [\hat{P}_{f,n}] \\
&= \mathbb{E}_{\hat{I}_n} \left[\int_{\mathcal{X}} \hat{I}_n(\mathbf{x}) f_{\mathbf{X}}(\mathbf{x}) d\mathbf{x} \right] \\
&= \int_{\mathcal{X}} \mathbb{E}_{\hat{I}_n} [\hat{I}_n(\mathbf{x})] f_{\mathbf{X}}(\mathbf{x}) d\mathbf{x} \\
&= \int_{\mathcal{X}} m_{\hat{I}_n}(\mathbf{x}) f_{\mathbf{X}}(\mathbf{x}) d\mathbf{x} \\
&= \int_{\mathcal{X}} \Phi \left(-\frac{m_{\hat{g}_n}(\mathbf{x})}{\sigma_{\hat{g}_n}(\mathbf{x})} \right) f_{\mathbf{X}}(\mathbf{x}) d\mathbf{x},
\end{aligned} \tag{13}$$

$$\begin{aligned}
\sigma_{\hat{P}_{f,n}}^2 &= \mathbb{V}_{\hat{I}_n} [\hat{P}_{f,n}] \\
&= \mathbb{E}_{\hat{I}_n} \left[\left(\hat{P}_{f,n} - \mathbb{E}_{\hat{I}_n} [\hat{P}_{f,n}] \right)^2 \right] \\
&= \mathbb{E}_{\hat{I}_n} \left[\left(\int_{\mathcal{X}} \hat{I}_n(\mathbf{x}) f_{\mathbf{X}}(\mathbf{x}) d\mathbf{x} - \int_{\mathcal{X}} \mathbb{E}_{\hat{I}_n} [\hat{I}_n(\mathbf{x})] f_{\mathbf{X}}(\mathbf{x}) d\mathbf{x} \right)^2 \right] \\
&= \mathbb{E}_{\hat{I}_n} \left[\left(\int_{\mathcal{X}} \left(\hat{I}_n(\mathbf{x}) - \mathbb{E}_{\hat{I}_n} [\hat{I}_n(\mathbf{x})] \right) f_{\mathbf{X}}(\mathbf{x}) d\mathbf{x} \right)^2 \right] \\
&= \mathbb{E}_{\hat{I}_n} \left[\left(\int_{\mathcal{X}} \left(\hat{I}_n(\mathbf{x}) - \mathbb{E}_{\hat{I}_n} [\hat{I}_n(\mathbf{x})] \right) f_{\mathbf{X}}(\mathbf{x}) d\mathbf{x} \right) \times \left(\int_{\mathcal{X}} \left(\hat{I}_n(\mathbf{x}') - \mathbb{E}_{\hat{I}_n} [\hat{I}_n(\mathbf{x}')] \right) f_{\mathbf{X}}(\mathbf{x}') d\mathbf{x}' \right) \right] \\
&= \mathbb{E}_{\hat{I}_n} \left[\int_{\mathcal{X}} \int_{\mathcal{X}} \left(\hat{I}_n(\mathbf{x}) - \mathbb{E}_{\hat{I}_n} [\hat{I}_n(\mathbf{x})] \right) \left(\hat{I}_n(\mathbf{x}') - \mathbb{E}_{\hat{I}_n} [\hat{I}_n(\mathbf{x}')] \right) f_{\mathbf{X}}(\mathbf{x}) f_{\mathbf{X}}(\mathbf{x}') d\mathbf{x} d\mathbf{x}' \right] \\
&= \int_{\mathcal{X}} \int_{\mathcal{X}} \mathbb{E}_{\hat{I}_n} \left[\left(\hat{I}_n(\mathbf{x}) - \mathbb{E}_{\hat{I}_n} [\hat{I}_n(\mathbf{x})] \right) \left(\hat{I}_n(\mathbf{x}') - \mathbb{E}_{\hat{I}_n} [\hat{I}_n(\mathbf{x}')] \right) \right] f_{\mathbf{X}}(\mathbf{x}) f_{\mathbf{X}}(\mathbf{x}') d\mathbf{x} d\mathbf{x}' \\
&= \int_{\mathcal{X}} \int_{\mathcal{X}} k_{\hat{I}_n}(\mathbf{x}, \mathbf{x}') f_{\mathbf{X}}(\mathbf{x}) f_{\mathbf{X}}(\mathbf{x}') d\mathbf{x} d\mathbf{x}',
\end{aligned} \tag{14}$$

175 where $\mathbb{E}_{\hat{I}_n} [\cdot]$ and $\mathbb{V}_{\hat{I}_n} [\cdot]$ denote expectation and variance operators taken over \hat{I}_n respectively. For compu-
176 tational purposes, Eq. (14) is further simplified by considering its upper bound. According to the Cauchy-
177 Schwarz inequality ($k_{\hat{I}_n}(\mathbf{x}, \mathbf{x}') \leq \sigma_{\hat{I}_n}(\mathbf{x}) \sigma_{\hat{I}_n}(\mathbf{x}')$), an upper-bound of the posterior variance (UPV) $\sigma_{\hat{P}_{f,n}}^2$ is
178 given as [43]:

$$\sigma_{\hat{P}_{f,n}}^2 \leq \bar{\sigma}_{\hat{P}_{f,n}}^2 = \left(\int_{\mathcal{X}} \sqrt{\Phi \left(-\frac{m_{\hat{g}_n}(\mathbf{x})}{\sigma_{\hat{g}_n}(\mathbf{x})} \right) \Phi \left(\frac{m_{\hat{g}_n}(\mathbf{x})}{\sigma_{\hat{g}_n}(\mathbf{x})} \right)} f_{\mathbf{X}}(\mathbf{x}) d\mathbf{x} \right)^2, \tag{15}$$

179 where the equality holds when the correlation of \hat{I}_n between any two locations $(\mathbf{x}, \mathbf{x}')$ is always equal to 1,
180 and $\bar{\sigma}_{\hat{P}_{f,n}}^2$ denotes the upper-bound of the posterior variance.

181 At the theoretical level, ALPI provides two important benefits. First, it offers a principled approach to
182 the quantification and propagation of numerical uncertainty via computation within the Bayesian framework.
183 Second, it gives the possibility to reduce the numerical uncertainty by using an active learning strategy (see
184 next subsection).

185 *2.2. Numerical algorithm*

186 **For practical reliability analysis**, the failure probability estimate should be inferred using as few obser-
187 vations as possible, with the premise of limiting its numerical uncertainty within a pre-specified tolerance.
188 Besides, as the posterior mean and UPV of failure probability (Eqs. (13) and (15)) lack of closed-form solu-
189 tions, a numerical integrator is necessary to make the method practically feasible. The numerical algorithm
190 of the ALPI method for failure probability estimation is summarized in [Appendix A](#).

191 When it comes to numerical implementation, ALPI shows two main limitations. First, it is not applicable
192 to problems with extremely small failure probabilities (typically, less than 10^{-4}) as a large number of
193 Monte Carlo (MC) samples (typically, more than 10^6) are required, making each iteration computationally
194 cumbersome and even infeasible. Second, it is not suitable for parallel computing since only one point
195 is identified at each iteration, resulting in a waste of useful information and computational resources for
196 engineering applications.

197 **3. Parallel adaptive Bayesian quadrature**

198 The major limitations of ALPI at implementation level will be addressed in this section. Further, a novel
199 method, called ‘Parallel Adaptive Bayesian Quadrature’ (PABQ), is presented on the theoretical basis of
200 ALPI. As its name indicates, the proposed PABQ method can support parallel distributed processing. Most
201 importantly, PABQ is able to estimate very small failure probabilities (e.g., 10^{-7}).

202 *3.1. General remarks*

203 As we did not imply any distribution types for \mathbf{X} when making Bayesian inference about the failure
204 probability in the last section, it means that the ALPI framework is naturally applicable in the stan-
205 dard normal space. In view of this, let us transform $g(\mathbf{x})$ from the physical space \mathcal{X} to the standard
206 normal space \mathcal{U} , i.e., $g(\mathbf{x}) = g(T^{-1}(\mathbf{u})) = \mathcal{G}(\mathbf{u})$, where \mathbf{u} is a realization of the standard normal vector
207 $\mathbf{U} = [U_1, U_2, \dots, U_d] \in \mathcal{U} \subseteq \mathbb{R}^d$ and T^{-1} is the inverse transformation (e.g., iso-probabilistic, Nataf, and
208 Rosenblatt transformation, etc.). For clarification, the transformed performance function is denoted as
209 $Z = \mathcal{G}(\mathbf{U})$. Different from ALPI, the proposed PABQ method will be implemented with the $\mathcal{G} = g \circ T^{-1}$ -
210 function.

211 *3.2. Importance ball sampling*

212 In this subsection, we propose an importance ball sampling (IBS) technique to replace the MC method
213 used in the conventional ALPI method. Let us first introduce a ball, a region enclosed by a sphere or
214 hypersphere. The d -ball of radius $r > 0$ in the standard normal space \mathcal{U} can be defined as $B^d(r) =$
215 $\{\mathbf{u} \in \mathbb{R}^d : \|\mathbf{u}\|_2 \leq r\}$, where $\|\cdot\|_2$ denotes the 2-norm. The ball is said to be ‘important’ when it can cover

216 the standard normal space with relatively large probability content (in case that r is appropriately chosen).
 217 The uniform PDF over $B^d(r)$ takes the form:

$$f_B(\mathbf{u}) = \begin{cases} \frac{1}{V_d(r)}, & \text{if } \|\mathbf{u}\|_2 \leq r; \\ 0, & \text{otherwise} \end{cases}, \quad (16)$$

218 where $V_d(r) = \frac{\pi^{d/2}}{\Gamma(\frac{d}{2}+1)}r^d$ is the volume of $B^d(r)$, $\Gamma(\cdot)$ is Euler's gamma function. To generate random
 219 points uniformly distributed within the d -ball, there are many methods available in the literature. In this
 220 study, one algorithm reported in [62] is adopted, as summarized in Algorithm 1.

Algorithm 1 Generate uniform samples within the d -ball [62]

- 1: **Input:** dimension d , radius r and sample size N_{ibs}
 - 2: **for** $i = 1, 2, \dots, N_{ibs}$ **do**
 - 3: Generate d normally distributed samples, $\mathbf{w} = [w^{(1)}, w^{(2)}, \dots, w^{(d)}], w^{(i)} \sim \mathcal{N}(0, 1)$
 - 4: Generate a uniformly distributed sample v from the interval $[0, 1]$
 - 5: Return the i -th vector $\bar{\mathbf{u}}^{(i)} = \frac{rv^{1/d}\mathbf{w}}{\|\mathbf{w}\|_2}$
 - 6: **end for**
 - 7: **Output:** $\bar{\mathcal{U}} = \{\bar{\mathbf{u}}^{(i)}\}_{i=1}^{N_{ibs}}$: N_{ibs} uniform samples in $B^d(r)$
-

221 Then, consider an **auxiliary PDF** constructed as follows:

$$f_0(\mathbf{u}) = \begin{cases} (1 - \Delta) f_B(\mathbf{u}), & \|\mathbf{u}\|_2 \leq r \\ f_U(\mathbf{u}), & \text{otherwise} \end{cases}, \quad (17)$$

222 where $f_U(\mathbf{u})$ is the joint PDF of \mathbf{U} ; Δ is a normalizing constant that ensures that the PDF $f_0(\mathbf{u})$ integrates
 223 to one, which is actually equal to the probability of $f_U(\mathbf{u})$ outside $B^d(r)$, i.e., $\Delta = \int_{\mathcal{U} \setminus \mathcal{B}} f_U(\mathbf{u}) d\mathbf{u}$. The
 224 posterior mean $m_{\hat{P}_{f,n}}$ and upper-bound of posterior standard deviation (UPSTD) $\bar{\sigma}_{\hat{P}_{f,n}}$ with respect to the
 225 \mathcal{G} -function can be reformulated respectively as:

$$\begin{aligned} m_{\hat{P}_{f,n}} &= \int_{\mathcal{U}} \Phi\left(-\frac{m_{\hat{G}_n}(\mathbf{u})}{\sigma_{\hat{G}_n}(\mathbf{u})}\right) f_U(\mathbf{u}) d\mathbf{u} \\ &= \int_{\mathcal{U}} \Phi\left(-\frac{m_{\hat{G}_n}(\mathbf{u})}{\sigma_{\hat{G}_n}(\mathbf{u})}\right) \frac{f_U(\mathbf{u})}{f_0(\mathbf{u})} f_0(\mathbf{u}) d\mathbf{u} \\ &= \int_{\mathcal{B}} \Phi\left(-\frac{m_{\hat{G}_n}(\mathbf{u})}{\sigma_{\hat{G}_n}(\mathbf{u})}\right) \frac{f_U(\mathbf{u})}{(1 - \Delta) f_B(\mathbf{u})} (1 - \Delta) f_B(\mathbf{u}) d\mathbf{u} \\ &\quad + \int_{\mathcal{U} \setminus \mathcal{B}} \Phi\left(-\frac{m_{\hat{G}_n}(\mathbf{u})}{\sigma_{\hat{G}_n}(\mathbf{u})}\right) \frac{f_U(\mathbf{u})}{f_U(\mathbf{u})} f_U(\mathbf{u}) d\mathbf{u} \\ &= V_d(r) \int_{\mathcal{B}} \Phi\left(-\frac{m_{\hat{G}_n}(\mathbf{u})}{\sigma_{\hat{G}_n}(\mathbf{u})}\right) f_U(\mathbf{u}) f_B(\mathbf{u}) d\mathbf{u} \\ &\quad + \int_{\mathcal{U} \setminus \mathcal{B}} \Phi\left(-\frac{m_{\hat{G}_n}(\mathbf{u})}{\sigma_{\hat{G}_n}(\mathbf{u})}\right) f_U(\mathbf{u}) d\mathbf{u}, \end{aligned} \quad (18)$$

$$\begin{aligned}
\bar{\sigma}_{\hat{P}_{f,n}} &= \int_{\mathcal{U}} \sqrt{\Phi\left(-\frac{m_{\hat{\mathcal{G}}_n}(\mathbf{u})}{\sigma_{\hat{\mathcal{G}}_n}(\mathbf{u})}\right) \Phi\left(\frac{m_{\hat{\mathcal{G}}_n}(\mathbf{u})}{\sigma_{\hat{\mathcal{G}}_n}(\mathbf{u})}\right)} f_{\mathcal{U}}(\mathbf{u}) d\mathbf{u} \\
&= \int_{\mathcal{U}} \sqrt{\Phi\left(-\frac{m_{\hat{\mathcal{G}}_n}(\mathbf{u})}{\sigma_{\hat{\mathcal{G}}_n}(\mathbf{u})}\right) \Phi\left(\frac{m_{\hat{\mathcal{G}}_n}(\mathbf{u})}{\sigma_{\hat{\mathcal{G}}_n}(\mathbf{u})}\right) \frac{f_{\mathcal{U}}(\mathbf{u})}{f_0(\mathbf{u})}} f_0(\mathbf{u}) d\mathbf{u} \\
&= \int_{\mathcal{B}} \sqrt{\Phi\left(-\frac{m_{\hat{\mathcal{G}}_n}(\mathbf{u})}{\sigma_{\hat{\mathcal{G}}_n}(\mathbf{u})}\right) \Phi\left(\frac{m_{\hat{\mathcal{G}}_n}(\mathbf{u})}{\sigma_{\hat{\mathcal{G}}_n}(\mathbf{u})}\right) \frac{f_{\mathcal{U}}(\mathbf{u})}{(1-\Delta)f_B(\mathbf{u})}} (1-\Delta)f_B(\mathbf{u}) d\mathbf{u} \\
&\quad + \int_{\mathcal{U}\setminus\mathcal{B}} \sqrt{\Phi\left(-\frac{m_{\hat{\mathcal{G}}_n}(\mathbf{u})}{\sigma_{\hat{\mathcal{G}}_n}(\mathbf{u})}\right) \Phi\left(\frac{m_{\hat{\mathcal{G}}_n}(\mathbf{u})}{\sigma_{\hat{\mathcal{G}}_n}(\mathbf{u})}\right) \frac{f_{\mathcal{U}}(\mathbf{u})}{f_{\mathcal{U}}(\mathbf{u})}} f_{\mathcal{U}}(\mathbf{u}) d\mathbf{u} \\
&= V_d(r) \int_{\mathcal{B}} \sqrt{\Phi\left(-\frac{m_{\hat{\mathcal{G}}_n}(\mathbf{u})}{\sigma_{\hat{\mathcal{G}}_n}(\mathbf{u})}\right) \Phi\left(\frac{m_{\hat{\mathcal{G}}_n}(\mathbf{u})}{\sigma_{\hat{\mathcal{G}}_n}(\mathbf{u})}\right)} f_{\mathcal{U}}(\mathbf{u}) f_B(\mathbf{u}) d\mathbf{u} \\
&\quad + \int_{\mathcal{U}\setminus\mathcal{B}} \sqrt{\Phi\left(-\frac{m_{\hat{\mathcal{G}}_n}(\mathbf{u})}{\sigma_{\hat{\mathcal{G}}_n}(\mathbf{u})}\right) \Phi\left(\frac{m_{\hat{\mathcal{G}}_n}(\mathbf{u})}{\sigma_{\hat{\mathcal{G}}_n}(\mathbf{u})}\right)} f_{\mathcal{U}}(\mathbf{u}) d\mathbf{u},
\end{aligned} \tag{19}$$

226 where $m_{\hat{\mathcal{G}}_n}(\mathbf{u})$ and $\sigma_{\hat{\mathcal{G}}_n}(\mathbf{u})$ are the posterior mean and STD functions of \mathcal{G} conditional on n observations.
227 Note that if one chooses a sufficiently small Δ (i.e., r is sufficiently large), $f_{\mathcal{U}}(\mathbf{u})$ over $\mathcal{U}\setminus\mathcal{B}$ will approach to
228 zero. In this case, the last terms in both Eqs. (18) and (19) can be neglected, and hence $m_{\hat{P}_{f,n}}$ and $\bar{\sigma}_{\hat{P}_{f,n}}$
229 are approximately equal to:

$$m_{\hat{P}_{f,n}} \approx V_d(r) \int_{\mathcal{B}} \Phi\left(-\frac{m_{\hat{\mathcal{G}}_n}(\mathbf{u})}{\sigma_{\hat{\mathcal{G}}_n}(\mathbf{u})}\right) f_{\mathcal{U}}(\mathbf{u}) f_B(\mathbf{u}) d\mathbf{u}, \tag{20}$$

$$\bar{\sigma}_{\hat{P}_{f,n}} \approx V_d(r) \int_{\mathcal{B}} \sqrt{\Phi\left(-\frac{m_{\hat{\mathcal{G}}_n}(\mathbf{u})}{\sigma_{\hat{\mathcal{G}}_n}(\mathbf{u})}\right) \Phi\left(\frac{m_{\hat{\mathcal{G}}_n}(\mathbf{u})}{\sigma_{\hat{\mathcal{G}}_n}(\mathbf{u})}\right)} f_{\mathcal{U}}(\mathbf{u}) f_B(\mathbf{u}) d\mathbf{u}. \tag{21}$$

231 The above two equations are the basic of the proposed IBS method, and $f_B(\mathbf{u})$ is regarded as the importance
232 sampling density. The IBS estimators of Eqs. (20) and (21) are given as:

$$\tilde{m}_{\hat{P}_{f,n}} = \frac{V_d(r)}{N_{ibs}} \sum_{i=1}^{N_{ibs}} \Phi\left(-\frac{m_{\hat{\mathcal{G}}_n}(\bar{\mathbf{u}}^{(i)})}{\sigma_{\hat{\mathcal{G}}_n}(\bar{\mathbf{u}}^{(i)})}\right) f_{\mathcal{U}}(\bar{\mathbf{u}}^{(i)}), \tag{22}$$

$$\tilde{\sigma}_{\hat{P}_{f,n}} = \frac{V_d(r)}{N_{ibs}} \sum_{i=1}^{N_{ibs}} \sqrt{\Phi\left(-\frac{m_{\hat{\mathcal{G}}_n}(\bar{\mathbf{u}}^{(i)})}{\sigma_{\hat{\mathcal{G}}_n}(\bar{\mathbf{u}}^{(i)})}\right) \Phi\left(\frac{m_{\hat{\mathcal{G}}_n}(\bar{\mathbf{u}}^{(i)})}{\sigma_{\hat{\mathcal{G}}_n}(\bar{\mathbf{u}}^{(i)})}\right)} f_{\mathcal{U}}(\bar{\mathbf{u}}^{(i)}), \tag{23}$$

234 where $\bar{\mathbf{u}}^{(i)} \sim f_B(\mathbf{u})$. The variances of the estimators are formulated as follows:

$$\mathbb{V}[\tilde{m}_{\hat{P}_{f,n}}] = \frac{V_d^2(r)}{(N_{ibs}-1)N_{ibs}} \sum_{i=1}^{N_{ibs}} \left[\Phi\left(-\frac{m_{\hat{\mathcal{G}}_n}(\bar{\mathbf{u}}^{(i)})}{\sigma_{\hat{\mathcal{G}}_n}(\bar{\mathbf{u}}^{(i)})}\right) f_{\mathcal{U}}(\bar{\mathbf{u}}^{(i)}) - \tilde{m}_{\hat{P}_{f,n}} \right]^2, \tag{24}$$

$$\mathbb{V}[\tilde{\sigma}_{\hat{P}_{f,n}}] = \frac{V_d^2(r)}{(N_{ibs}-1)N_{ibs}} \sum_{i=1}^{N_{ibs}} \left[\sqrt{\Phi\left(-\frac{m_{\hat{\mathcal{G}}_n}(\bar{\mathbf{u}}^{(i)})}{\sigma_{\hat{\mathcal{G}}_n}(\bar{\mathbf{u}}^{(i)})}\right) \Phi\left(\frac{m_{\hat{\mathcal{G}}_n}(\bar{\mathbf{u}}^{(i)})}{\sigma_{\hat{\mathcal{G}}_n}(\bar{\mathbf{u}}^{(i)})}\right)} f_{\mathcal{U}}(\bar{\mathbf{u}}^{(i)}) - \tilde{\sigma}_{\hat{P}_{f,n}} \right]^2. \tag{25}$$

236 Similar to the MC population in ALPI, the population generated from $f_{\mathcal{B}}(\mathbf{u})$ also plays two roles. First,
 237 the posterior mean and UPSTD of the failure probability should be evaluated numerically based on those
 238 samples at each iteration, as shown in Eqs. (22) and (23). Second, it will be used as a candidate sample
 239 pool by which multiple promising points can be identified at each iteration (see next subsection).

240 Given dimension d , the IBS method has two parameters to be specified appropriately, i.e., radius r and
 241 simple size N_{ibs} . As we have mentioned, r should be large enough to ensure that Δ is small enough. By doing
 242 so, (1) the bias between Eqs. (20) and (18), and also Eqs. (21) and (19) can be neglected; (2) candidate
 243 samples can reach the failure domain characterized by a small probability. The probability of $f_{\mathcal{U}}(\mathbf{u})$ within
 244 the d -ball can be given as (see Appendix E of [63]):

$$F(d, r) = \frac{1}{\Gamma(d/2)} \int_0^{r^2/2} x^{d/2-1} \exp(-x) dx. \quad (26)$$

245 Based on this, r can be determined as the solution to:

$$F(d, r) = 1 - \Delta, \quad (27)$$

246 It should be noted that given a fixed Δ , r increases with d . For example, if we set Δ as 10^{-8} , $r \approx 6.07$ for
 247 $d = 2$, and $r \approx 6.77$ for $d = 5$. As for N_{ibs} , it cannot be too small otherwise the estimators of $m_{\hat{P}_{f,n}}$ and
 248 $\bar{\sigma}_{\hat{P}_{f,n}}$ will process relatively large variances, and also cannot fill the d -ball well. On the contrary, a too large
 249 N_{ibs} can lead to numerical difficulty and memory problems.

250 As an illustration, Fig. 1 shows two populations generated respectively by MC and IBS in two dimensions
 251 with the same sample size 10^5 . Obviously, the IBS method can produce a better space-filling population
 252 and cover a larger area than that of MC method. If one would like the MC population to cover as large
 253 space as the IBS population, the sample size should be increased many times ($> 10^3$).

254 3.3. Multi-point UPVC criterion

255 In order to enable parallel processing, a batch of informative points should be identified to evaluate on the
 256 \mathcal{G} -function at each iteration, rather than only one single point. For this purpose, we propose a multi-point
 257 UPVC criterion, which leverages the advantages of both the UPVC function [43] and k -means clustering
 258 [64].

259 Suppose that we have inferred a GP posterior $\hat{\mathcal{G}}_n \sim \mathcal{GP}(m_{\hat{\mathcal{G}}_n}(\mathbf{u}), k_{\hat{\mathcal{G}}_n}(\mathbf{u}, \mathbf{u}'))$ of \mathcal{G} at a certain step of the
 260 proposed PABQ method. Analogous to Eq. (A.3), the corresponding UPVC function can be defined as:

$$\text{UPVC}(\mathbf{u}) = \sqrt{\Phi\left(-\frac{m_{\hat{\mathcal{G}}_n}(\mathbf{u})}{\sigma_{\hat{\mathcal{G}}_n}(\mathbf{u})}\right) \Phi\left(\frac{m_{\hat{\mathcal{G}}_n}(\mathbf{u})}{\sigma_{\hat{\mathcal{G}}_n}(\mathbf{u})}\right)} \times f_{\mathcal{U}}(\mathbf{u}), \quad (28)$$

261 where $\sigma_{\hat{\mathcal{G}}_n}(\mathbf{u}) = \sqrt{k_{\hat{\mathcal{G}}_n}(\mathbf{u}, \mathbf{u})}$ is the posterior STD function of \mathcal{G} . Note that $\bar{\sigma}_{\hat{P}_{f,n}}^2 = [\int_{\mathcal{U}} \text{UPVC}(\mathbf{u}) d\mathbf{u}]^2$
 262 holds, and hence the UPVC function is a measure of the contribution of numerical uncertainty at the point

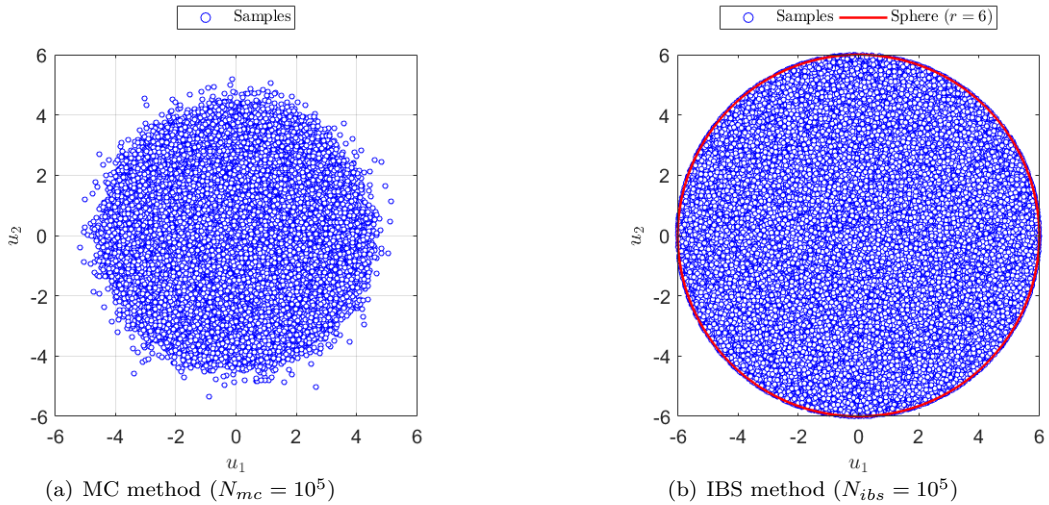


Figure 1: Comparison between MC and IBS methods in two dimensions.

263 \mathbf{u} to the UPV of the failure probability. The traditional UPVC criterion, however, only selects the point
 264 among a MC population that has the maximum UPVC value as the best next point to evaluate on the \mathcal{G} -
 265 function. As such, other information provided by the UPVC function that might be still useful is discarded
 266 at each iteration. This drawback can be alleviated by identifying multiple points. The conventional k -means
 267 clustering technique can be used to partition $\overline{\mathcal{U}}$ into k clusters, but it cannot take the UPVC measure into
 268 account. In this study, a weighted clustering algorithm is proposed by combining the UPVC function with
 269 k -means clustering, which is referred as ‘UPVC-weighted k -means clustering’. Suppose that we wish to
 270 select q points among $\overline{\mathcal{U}}$ at each iteration, and hence evaluation of the \mathcal{G} -function at these q points can
 271 be distributed on q processors simultaneously. The number of points q also corresponds to the number of
 272 clusters. A compact pseudocode of the proposed algorithm is given in Algorithm 2. The selected q points
 273 correspond to the q centroids produced by the proposed UPVC-weighted k -means clustering. It should be
 274 pointed out that the identified points usually do not belong to $\overline{\mathcal{U}}$ any more due to the weighted averaging
 275 operator embedded in the proposed algorithm.

276 A test example is considered here to illustrate the proposed multi-point UPVC criterion. The performance
 277 function is given as $Z = \mathcal{G}(\mathbf{U}) = U_1^2 - U_2 + 2$, where U_1 and U_2 are two independent standard normal variables.
 278 For reproducibility, we specify the initial observed locations as $\mathcal{U} = \{(-\sqrt{5}, 0), (0, 0), (\sqrt{5}, 0), (0, -\sqrt{5}), (0, \sqrt{5})\}$.
 279 Based on these five initial observations, we can obtain a posterior GP over the \mathcal{G} -function and also the UPVC
 280 function. Additional $q = 5$ points are then identified by the proposed UPVC-weighted k -means clustering
 281 algorithm from 10^5 uniform samples within the 2-ball of $r = 6$. As shown in Fig. 2, the newly selected points
 282 are sparsely located in areas where the UPVC values are not very small. Therefore, the total information
 283 gained from those 5 points could be more than that of the one with the maximum UPVC value.

Algorithm 2 UPVC-weighted k -means clustering algorithm

Input: the number of clusters q , UPVC(\mathbf{u}) and $\overline{\mathcal{U}}$

1. **Initialization.** Randomly select q points among $\overline{\mathcal{U}}$ as the initial centroids, denoted by $\mathbf{E}^{(1)} = \{\mathbf{e}^{(i)}\}_{i=1}^q$;

2. **Assignment step.** Each point among $\overline{\mathcal{U}}$ is assigned to a cluster for which the squared Euclidean distance between the point and the cluster centroid is shortest. The i -th cluster is denoted as $\mathcal{C}^{(i)} = \{\mathbf{c}_j^{(i)}\}_{j=1}^{N_i}$, where $\mathbf{c}_j^{(i)}$ is the j -th point in the i -th cluster ($j = 1, 2, \dots, N_i$);

3. **Update step.** Each centroid is then updated by UPVC-weighted mean of the cluster:

$$\mathbf{e}^{(i)} = \frac{\sum_{j=1}^{N_i} \text{UPVC}(\mathbf{c}_j^{(i)}) \times \mathbf{c}_j^{(i)}}{\sum_{j=1}^{N_i} \text{UPVC}(\mathbf{c}_j^{(i)})}$$

4. **Iteration.** Repeat the assignment step and update step until the centroids do not change or the predefined number of iterations is reached.

Output: q centroids

284 *3.4. Summary of the proposed method*

285 The numerical implementation procedure of the proposed PABQ method for reliability analysis, which
 286 is also shown in Fig. 3, consists of the following main steps:

287

288 **Step B.1: Generate uniformly distributed samples within the d -ball**

289 Generate N_{ibs} uniform samples within the d -ball of radius r , using Algorithm 1, denoted as $\overline{\mathcal{U}} =$
 290 $\{\overline{\mathbf{u}}^{(i)}\}_{i=1}^{N_{ibs}}$.

291 **Step B.2: Get initial observations**

292 Randomly select N_0 samples among $\overline{\mathcal{U}}$, denoted by $\mathcal{U} = \{\mathbf{u}^{(i)}\}_{i=1}^{N_0}$. These samples are evaluated on the

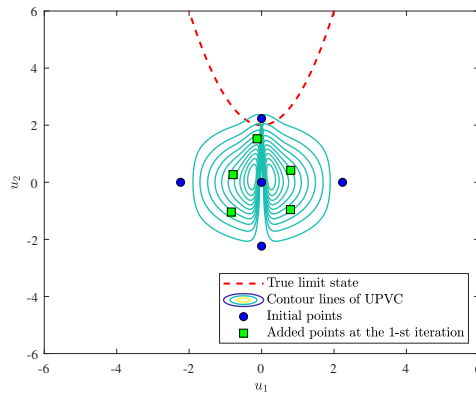


Figure 2: Illustration of the proposed multi-points UPVC criterion by a test example.

293 \mathcal{G} -function in parallel to obtain the corresponding observations $\mathcal{Z} = \{z^{(i)}\}_{i=1}^{N_0}$ ($z^{(i)} = \mathcal{G}(\mathbf{u}^{(i)})$). The initial
 294 dataset is constructed by $\mathcal{D} = \{\mathcal{U}, \mathcal{Z}\}$. Let $n = N_0$.

295 **Step B.3: Make Bayesian inference about the failure probability**

296 By assigning a GP prior for the \mathcal{G} -function, we finally arrive at the posterior mean and UPSTD of the fail-
 297 ure probability conditional on \mathcal{D} . In this study, the prior mean and covariance of $\hat{\mathcal{G}}_0 \sim \mathcal{GP}(m_{\hat{\mathcal{G}}_0}(\mathbf{x}), k_{\hat{\mathcal{G}}_0}(\mathbf{x}, \mathbf{x}'))$
 298 are assumed to be a constant and the squared exponential kernel respectively. The involved hyper-parameters
 299 are tuned by using the maximum likelihood estimation, and this stage is implemented with the *fitrgp* func-
 300 tion in Statistics and Machine Learning Toolbox of Matlab. The posterior mean and UPSTD of the failure
 301 probability are then evaluated based on Eqs. (22) and (23).

302 **Step B.4: Check the stopping criterion**

303 If $\frac{\tilde{\sigma}_{\hat{P}_{f,n}}}{\tilde{m}_{\hat{P}_{f,n}}} < \epsilon$ is satisfied, go to **Step B.6**; Else, go to **Step B.5**. Here $\frac{\tilde{\sigma}_{\hat{P}_{f,n}}}{\tilde{m}_{\hat{P}_{f,n}}}$ denotes the estimated
 304 upper-bound of the posterior COV of the failure probability, and ϵ is a user-specified threshold.

305 **Step B.5: Enrich the previous dataset**

306 Identify additional q points by using the proposed multi-point UPVC criterion (see Algorithm 2), denoted
 307 by $\mathcal{U}_+ = \{\mathbf{u}_+^{(i)}\}_{i=1}^q$. Then, the corresponding observations of the \mathcal{G} -function at those q identified points \mathcal{U}_+
 308 should be obtained using parallel computing, denoted by $\mathcal{Z}_+ = \{z_+^{(i)}\}_{i=1}^q$ with $z_+^{(i)} = \mathcal{G}(\mathbf{u}_+^{(i)})$. The previous
 309 dataset \mathcal{D} is enriched with $\mathcal{D}_+ = \{\mathcal{U}_+, \mathcal{Z}_+\}$, i.e., $\mathcal{D} = \mathcal{D} \cup \mathcal{D}_+$. Let $n = n + q$, and go to **Step B.3**.

310 **Step B.6: End the algorithm**

311 Return $\tilde{m}_{\hat{P}_{f,n}}$ as the estimated failure probability and end the algorithm.

312
 313 For practical implementation, it is necessary to set proper values for constants N_{ibs} , r , N_0 , ϵ and q .
 314 The selection of these parameters is problem-dependent. However, according to our experience some general
 315 guidelines for selecting them are the following: $N_{ibs} = 5 \times 10^5 \sim 1 \times 10^6$, $r = 6$, $N_0 = 10$, $\epsilon = 5\% \sim 10\%$
 316 and $q =$ the number of available processors for parallel computing.

317 **4. Numerical examples**

318 The performance of the proposed PABQ method is investigated by means of four numerical examples with
 319 varying complexity in this section. Several different parameter settings of PABQ are experimented in each
 320 example to study their effect on the results. For comparison, several state-of-the-art methods, i.e., FORM
 321 [65], SORM [65], AK-MCS [37], ALPI [43], AK-MCMC [46] and Polynomial-Chaos Kriging (PC-Kriging)
 322 [66], are also implemented when applicable.

323 *4.1. Example 1: A series system with four branches*

324 The first numerical example consists of a series system with four branches, which has been a classical
 325 benchmark example in structural reliability analysis (see, e.g., [67, 37, 68]). The performance function is

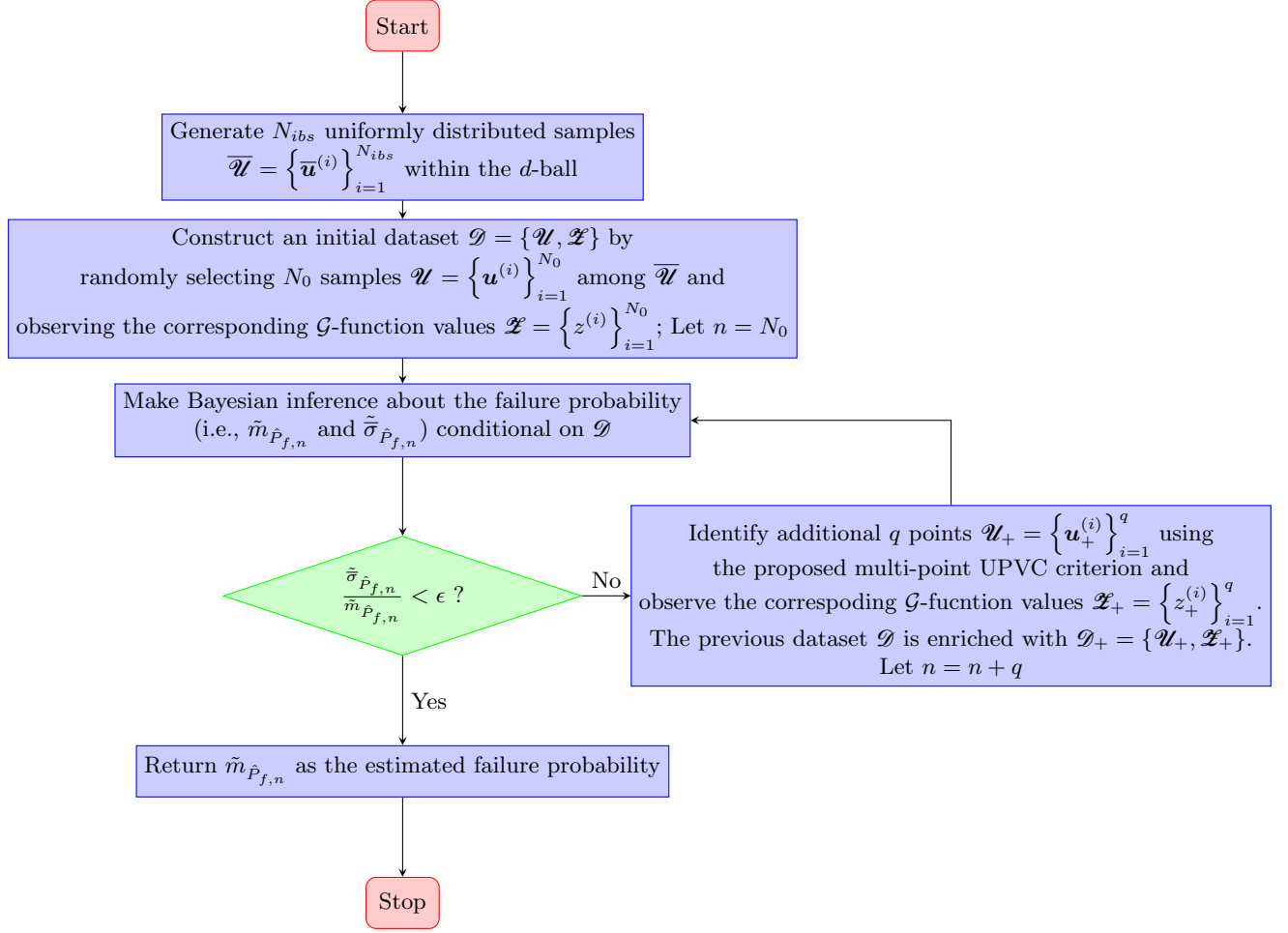


Figure 3: Flowchart of the proposed PABQ method.

326 given by:

$$Y = g(X_1, X_2) = \min \begin{cases} a + \frac{(X_1 - X_2)^2}{10} - \frac{(X_1 + X_2)}{\sqrt{2}}; \\ a + \frac{(X_1 - X_2)^2}{10} + \frac{(X_1 + X_2)}{\sqrt{2}}; \\ (X_1 - X_2) + \frac{b}{\sqrt{2}}; \\ (X_2 - X_1) + \frac{b}{\sqrt{2}} \end{cases}, \quad (29)$$

327 where X_1 and X_2 are two i.i.d. standard normal variables; a and b are two constant parameters. In this
 328 example, two cases by varying those two constant parameters are considered, where $a = 3$, $b = 6$ for the
 329 first case, and $a = 5$, $b = 10$ for the second case.

330 4.1.1. Results of Case I

331 In this case, the proposed PABQ method is compared to several other methods, i.e., AK-MCS+U [37],
 332 ALPI [43] and PC-Kriging [66]. Table 1 summarizes the results given as the number of iterations N_{iter} , the

333 total number of performance function calls N_{call} , the estimated failure probability \hat{P}_f , and the COV of \hat{P}_f
334 (i.e., $\text{COV}[\hat{P}_f]$). As seen, the proposed method with different q only takes a very few iterations in average
335 to converge, which are less than that of PC-Kriging, and far less than that of AK-MCS+U and ALPI. This
336 indicates that the proposed method could offer significant time savings when parallel computing is available.
337 Furthermore, the computational advantage may still exist even in case of non-parallel computing since the
338 average number of performance function calls is also reduced a lot by using the proposed method, especially
339 when q is small (e.g., $q = 6$). The results of \hat{P}_f and $\text{COV}[\hat{P}_f]$ also imply that the proposed method has an
340 accuracy similar to other methods being compared. By increasing N_{ibs} from 5×10^5 to 1×10^6 and decreasing
341 ϵ from 10% to 8%, the PABQ method can slightly reduce the COVs of failure probability estimates, at the
342 cost of marginally increased computation in an average sense.

343 To illustrate the proposed method visually, Fig. 4(a) depicts the points selected at two stages of an
344 exemplary run, as well as the true limit state curve. It is shown that most of the added points are sparsely
345 located, and some of them are close to the four important parts of the limit state curve that are crucial for
346 accurate failure probability estimation. These results indicate the effectiveness of the proposed multi-point
347 selection strategy.

Table 1: Reliability results for Example 1 (Case I).

Method		N_{iter}	N_{call}	\hat{P}_f	$\text{COV}[\hat{P}_f]/\%$
MCS		-	10^8	4.46×10^{-3}	0.15
AK-MCS+U		$1 + 96.55 = 97.55$	$12 + 96.55 = 108.55$	4.44×10^{-3}	1.54
ALPI		$1 + 72.95 = 73.95$	$12 + 72.95 = 84.95$	4.44×10^{-3}	1.79
PC-Kriging [66]	$q = 6$	$1 + 14.40 = 15.40$	$12 + 86.40 = 98.40$	4.46×10^{-3}	1.50
	$q = 6$	$1 + 5.60 = 6.60$	$10 + 33.60 = 43.60$	4.44×10^{-3}	2.53
	$q = 10$	$1 + 4.20 = 5.20$	$10 + 42.00 = 52.00$	4.40×10^{-3}	2.22
Proposed PABQ ($N_{ibs} = 5 \times 10^5, \epsilon = 10\%$)	$q = 15$	$1 + 3.65 = 4.65$	$10 + 54.75 = 64.75$	4.44×10^{-3}	1.35
	$q = 20$	$1 + 3.05 = 4.05$	$10 + 61.00 = 71.00$	4.44×10^{-3}	1.29
	$q = 6$	$1 + 8.64 = 9.64$	$10 + 43.20 = 53.20$	4.43×10^{-3}	2.17
	$q = 10$	$1 + 4.55 = 5.55$	$10 + 45.50 = 55.50$	4.40×10^{-3}	1.25
Proposed PABQ ($N_{ibs} = 1 \times 10^6, \epsilon = 8\%$)	$q = 15$	$1 + 3.70 = 4.70$	$10 + 55.50 = 65.50$	4.43×10^{-3}	1.02
	$q = 20$	$1 + 3.45 = 4.45$	$10 + 69.00 = 79.00$	4.45×10^{-3}	0.91

Note: For AK-MCS+U and ALPI, the MC population size is set as 10^6 . AK-MCS+U, ALPI and PABQ are performed 20 independent runs. PC-Kriging was performed 50 independent runs. Thus, for those methods, average results are reported for N_{iter} , N_{call} , and \hat{P}_f . Besides, $\text{COV}[\hat{P}_f]$ is also approximated accordingly.

348 *4.1.2. Results of Case II*

349 The failure probability is quite small (in the order of 10^{-7}) in Case II, and hence some methods, like
 350 AK-MCS and ALPI, are not applicable anymore. For this reason, the proposed method is mainly compared
 351 with AK-MCMC [46], which is capable of assessing extremely small failure probabilities. As can be seen
 352 from Table 2, the proposed method can not only reduce the average number of iterations greatly (especially
 353 when q is large, e.g., $q = 20$), but also the total number of calls to the performance function (especially
 354 when q is small, e.g., $q = 5$), in comparison to AK-MCMC. Besides, the proposed PABQ method is also
 355 able to yield fairly good average results for the failure probability. **It is noted that the COVs of the failure**
 356 **probability estimates can be reduced by a more strict parameter setting (i.e., $N_{ibs} = 1 \times 10^6, \epsilon = 8\%$).**
 357 This case study demonstrates the efficiency and accuracy of the proposed method for such a case with an
 358 extremely rare failure event.

Table 2: Reliability results for Example 1 (Case II).

Method	N_{iter}	N_{call}	\hat{P}_f	COV $[\hat{P}_f]/\%$
MCS	-	10^9	8.84×10^{-7}	3.36
AK-MCMC	$1 + 134.00 = 135.00$	$12 + 134.00 = 146.00$	8.85×10^{-7}	1.62
Proposed PABQ ($N_{ibs} = 5 \times 10^5, \epsilon = 10\%$)	$q = 5$ $1 + 8.80 = 9.80$	$10 + 44.00 = 54.00$	8.82×10^{-7}	2.14
	$q = 10$ $1 + 5.45 = 6.45$	$10 + 54.50 = 64.50$	8.84×10^{-7}	2.06
	$q = 15$ $1 + 4.75 = 5.75$	$10 + 71.25 = 81.25$	8.83×10^{-7}	1.24
	$q = 20$ $1 + 4.40 = 5.40$	$10 + 88.00 = 98.00$	8.88×10^{-7}	1.24
Proposed PABQ ($N_{ibs} = 1 \times 10^6, \epsilon = 8\%$)	$q = 5$ $1 + 8.80 = 9.80$	$10 + 44.00 = 54.00$	8.80×10^{-7}	1.63
	$q = 10$ $1 + 5.95 = 6.95$	$10 + 59.50 = 69.50$	8.83×10^{-7}	0.89
	$q = 15$ $1 + 4.95 = 5.95$	$10 + 74.25 = 84.25$	8.86×10^{-7}	0.89
	$q = 20$ $1 + 4.80 = 5.80$	$10 + 96.00 = 106.00$	8.86×10^{-7}	0.66

Note: AK-MCMC and PABQ are performed 20 independent runs. Thus, for those methods, average results are reported for N_{iter} , N_{call} , and \hat{P}_f . Besides, COV $[\hat{P}_f]$ is also approximated accordingly.

359 Fig. 4(b) depicts the points selected at two stages of the proposed method ($q = 10$) via an exemplary
 360 run, along with the real limit state curve. It is encouraging to see that the added points are relatively
 361 sparsely distributed, and most of them are located in the vicinity of true limit state curve.

362 *4.2. Example 2: A nonlinear oscillator*

363 A nonlinear undamped single-degree-of-freedom (SDOF) oscillator subjected to a rectangular pulse load
 364 [43] is adopted as the second example, as shown in Fig. 5. The performance function is defined as:

$$Y = g(m, c_1, c_2, r, F_1, t_1) = 3r - \left| \frac{2F_1}{c_1 + c_2} \sin \left(\frac{t_1}{2} \sqrt{\frac{c_1 + c_2}{m}} \right) \right|, \quad (30)$$

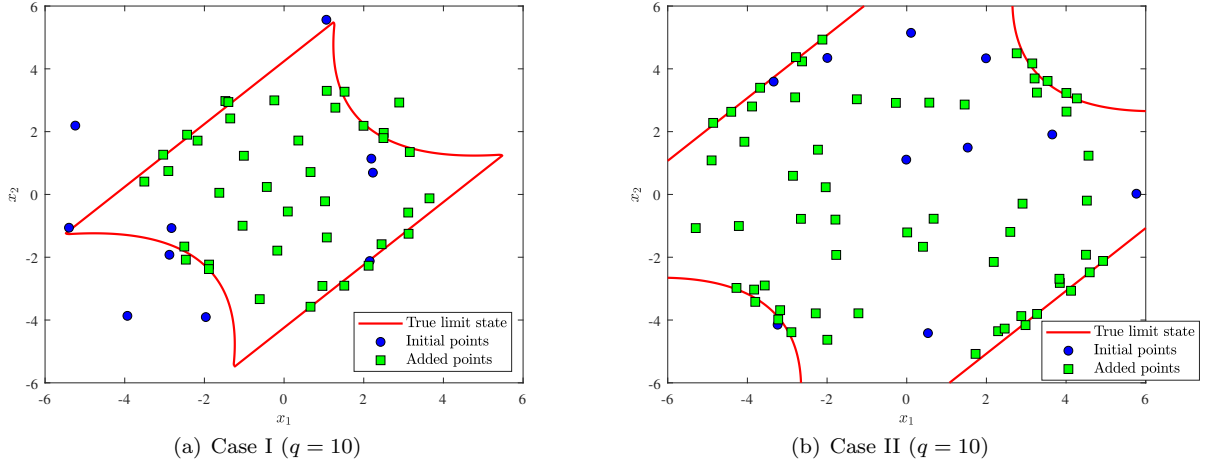


Figure 4: Points selected at different stages by the proposed PABQ method for Example 2.

where m, c_1, c_2, r, F_1, t_1 are six random variables, as described in Table 3.

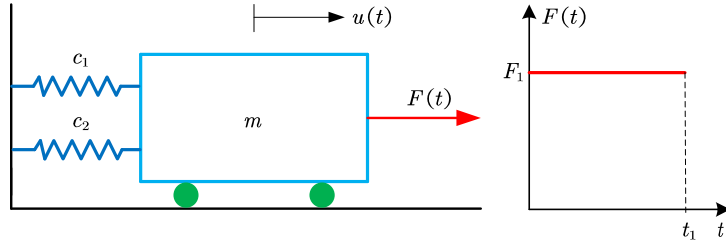


Figure 5: A nonlinear undamped SDOF oscillator subjected to pulse load.

The reference value of the failure probability is 5.17×10^{-6} (with COV being small, i.e., 1.39%), provided by MCS with 10^9 samples. As the failure probability is quite small, the proposed method is only compared to FORM [65], SORM [65] and AK-MCMC [46]. As can be seen from Table 4, the required average number of iterations by the proposed method is less than all the methods being compared, especially for AK-MCMC. This implies the parallel computing advantage of the proposed method. Besides, the proposed method is still more advantageous than FORM, SORM and AK-MCMC in computational efficiency in case of non-parallel computing, since the average number of performance function evaluations can also be reduced a lot (especially when q is small, e.g., $q = 5$). Although $\text{COV}[\hat{P}_f]$ given by the proposed method ($N_{ibs} = 5 \times 10^5, \epsilon = 10\%$) is around 5%, it can still be acceptable in practical applications. If one would like to reduce $\text{COV}[\hat{P}_f]$, one can increase N_{ibs} and decrease ϵ . For example, the last four rows of Table 4 give the results by of PABQ ($N_{ibs} = 1 \times 10^6, \epsilon = 5\%$). It can be seen that $\text{COV}[\hat{P}_f]$ is reduced to about 3% at the expense of increased N_{iter} and N_{call} in some cases ($q = 5, 10, 20$), while still much less than those of FORM, SORM and AK-MCMC.

Table 3: Random variables for Example 2.

Variable	Distribution	Mean	STD
m	Normal	1.0	0.05
c_1	Lognormal	1.0	0.10
c_2	Lognormal	0.1	0.01
r	Normal	0.5	0.05
F_1	Lognormal	0.5	0.10
t_1	Normal	1.0	0.20

379 4.3. Example 3: A simple bracket model

380 A simple bracket model that is available in the Partial Differential Equation Toolbox of Matlab is
381 considered as the third example. The schematic diagram of the bracket is shown in Figs. 6(a) and 6(b),
382 and more details of the model can be found in the description in the toolbox. The bracket is fixed at the
383 back face (face 4) and subjected to a distributed load in the negative z -direction in the front face (face
384 8). It is assumed that the Young's modulus E , Poisson's ratio μ , distributed load q and thickness h of the
385 horizontal plate with hole are characterized as independent random variables, whose statistical information
386 is summarized in Table. 5. The 10-node tetrahedral element is used to discretize the model, as shown in
387 Figs. 6(c) and 6(d). The maximal deflection of the bracket in the z direction is of concern in this example.
388 The limit state function is defined as:

$$Y = G(E, \mu, q, h) = \Delta - \bar{V}(E, \mu, q, h), \quad (31)$$

389 where Δ is the deterministic threshold, which is specified as $\Delta = 140 \mu\text{m}$; \bar{V} denotes the maximum dis-
390 placement of the bracket in the z -direction.

391 We implement several methods to assess the failure probability corresponding to the limit state function
392 defined in Eq. (31). The results are reported in Table 6. FORM does not converge within 100 iterations, so
393 its results are not included. The reference value of the failure probability is taken as the average result of
394 AK-MCMC, i.e., 1.90×10^{-6} (with a COV of 1.15%). It can be seen from Table 6 that the proposed PABQ
395 method can significantly reduce the number of iterations N_{iter} compared to AK-MCMC, while maintaining
396 reasonable accuracy. This indicates that our method could greatly outperform AK-MCMC in terms of
397 computational efficiency when parallel computing is available. One can also notice that the proposed method
398 requires less performance function calls in average than AK-MCMC. Therefore, the proposed method could
399 be still more efficient than AK-MCMC in case that parallel computing is unavailable. The variability of the
400 failure probability estimate given by the proposed method can be reduced to a certain level by setting a
401 large N_{ibs} and a small ϵ .

Table 4: Reliability results for Example 2.

Method	N_{iter}	N_{call}	\hat{P}_f	$\text{COV}[\hat{P}_f]/\%$
MCS	-	10^9	5.17×10^{-6}	1.39
FORM	10	80	5.45×10^{-6}	-
SORM	10	160	5.25×10^{-6}	-
AK-MCMC	$1 + 109.20 = 110.20$	$12 + 109.20 = 121.20$	5.23×10^{-6}	0.69
Proposed PABQ ($N_{ibs} = 5 \times 10^5, \epsilon = 10\%$)	$q = 5$ $1 + 3.15 = 4.15$	$10 + 15.75 = 25.75$	5.19×10^{-6}	5.68
	$q = 10$ $1 + 2.05 = 3.05$	$10 + 20.50 = 30.50$	5.21×10^{-6}	4.30
	$q = 15$ $1 + 1.65 = 2.65$	$10 + 24.75 = 34.75$	5.17×10^{-6}	4.30
	$q = 20$ $1 + 1.70 = 2.70$	$10 + 34.00 = 44.00$	5.21×10^{-6}	4.79
Proposed PABQ ($N_{ibs} = 1 \times 10^6, \epsilon = 5\%$)	$q = 5$ $1 + 4.05 = 5.05$	$10 + 20.25 = 30.25$	5.15×10^{-6}	3.08
	$q = 10$ $1 + 2.40 = 3.40$	$10 + 24.00 = 34.00$	5.15×10^{-6}	2.41
	$q = 15$ $1 + 2.00 = 3.00$	$10 + 30.00 = 40.00$	5.15×10^{-6}	3.53
	$q = 20$ $1 + 1.95 = 2.95$	$10 + 39.00 = 49.00$	5.20×10^{-6}	3.44

Note: AK-MCMC and PABQ are performed 20 independent runs. Thus, for those methods, average results are reported for N_{iter} , N_{call} , and \hat{P}_f . Besides, $\text{COV}[\hat{P}_f]$ is also approximated accordingly.

Table 5: Random variables for Example 3.

Variable	Distribution	Mean	COV
E (Gpa)	Lognormal	200	0.15
μ	Uniform	0.3	0.10
q (Pa)	Lognormal	10^4	0.20
h (mm)	Lognormal	10	0.10

4.4. Example 4: A 120-bar space truss structure

A 120-bar space truss structure [43], as shown in Fig. 7, is investigated in the last example to further demonstrate the proposed method. The structure is modelled as a three-dimensional (3D) finite-element model with 49 nodes and 120 elements in OpenSees. Nodes 0, 1, 4, 7 and 10 withstand concentrated loads along the negative z -axis, denoted as P_0, P_1, P_4, P_7 and P_{10} respectively. All elements are assumed to have the same cross-sectional area A and Young's modulus E . The structure is expected to be in a linear elastic state, so we simply employ linear finite element analysis. The performance function is defined as:

$$Y = g(P_0, P_1, P_4, P_7, A, E) = \Delta - V_{0,z}, \quad (32)$$

where $V_{0,z}$ denotes the vertical displacement of node 0; and Δ is the threshold, specified as 90 mm. The random variables considered in this examples are summarized in Table 7.

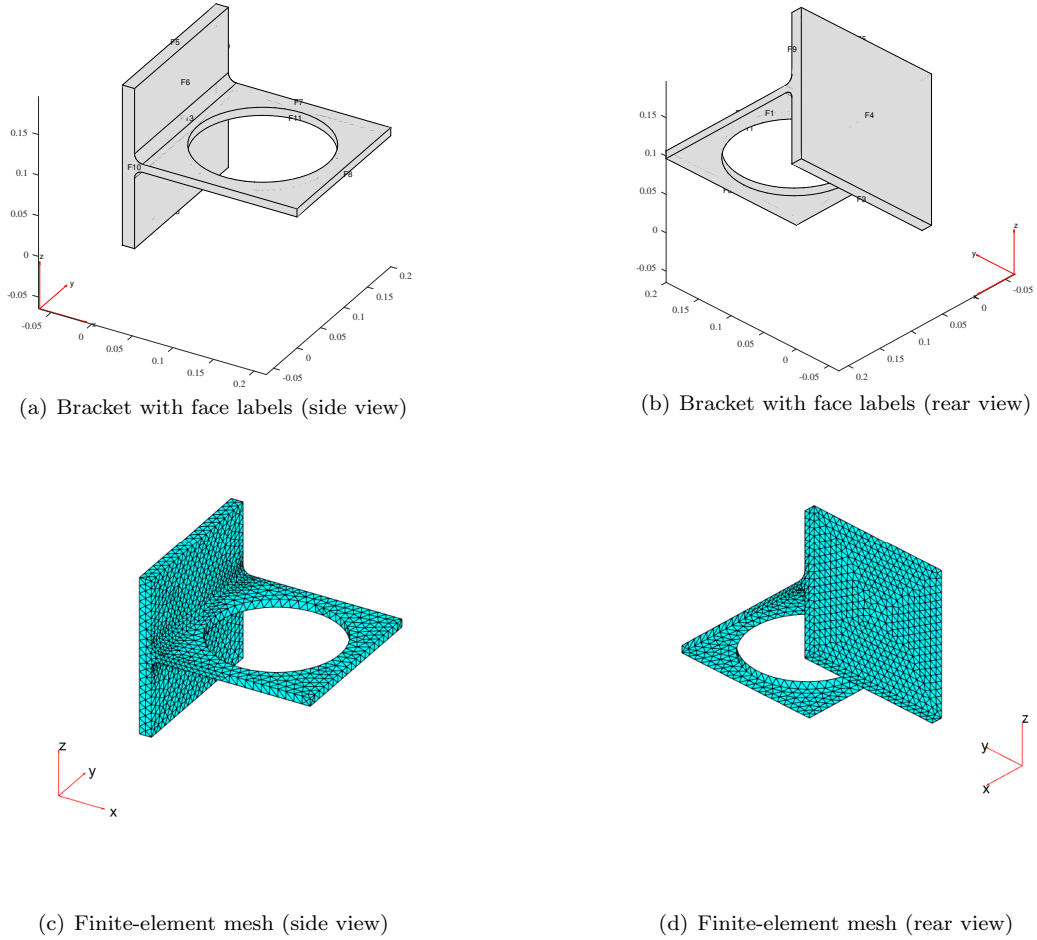


Figure 6: A simple bracket model: Geometry and finite-element mesh.

411 In this example, several methods, i.e., MCS, FORM [65], SORM [65], AK-MCS+U [37], ALPI [43], AK-
 412 MCMC [46] and PABQ, are implemented to assess the failure probability. The results are listed in Table 8.
 413 The reference value for the failure probability is 5.08×10^{-4} with COV being 4.44, provided by MCS with 10^6
 414 samples. The results of AK-MCMC are not reported because it fails to converge in multiple trials. FORM
 415 only requires 7 iterations and a total number of 65 performance function calls, which, however, results in an
 416 inaccurate result. SORM can provide more accurate failure probability estimate than FORM at the expense
 417 of 172 calls to the performance function (hence the finite-element model). Compared to AK-MCS+U and
 418 ALPI, the proposed PABQ method performs better in terms of N_{call} (especially when q is small, e.g., $q = 5$),
 419 and much better in terms of N_{iter} (especially when q is large, e.g., $q = 20$). This implies that PABQ can
 420 be much more efficient than AK-MCS+U and ALPI in cases of both parallel and non-parallel computing.
 421 Besides, the proposed method still has a acceptable accuracy, as indicated by \hat{P}_f and $COV[\hat{P}_f]$. As shown
 422 in the last four rows of Table 8, $COV[\hat{P}_f]$ can be further reduced by increasing N_{ibs} and decreasing ϵ at the

Table 6: Reliability results for Example 3.

Method	N_{iter}	N_{call}	\hat{P}_f	$\text{COV}[\hat{P}_f]/\%$
FORM	-	-	-	-
AK-MCMC	1 + 44.60 = 45.60	12 + 44.60 = 56.60	1.90×10^{-6}	1.15
	$q = 2$ 1 + 1.85 = 2.85	10 + 3.70 = 13.70	1.93×10^{-6}	4.99
	$q = 3$ 1 + 1.45 = 2.45	10 + 4.35 = 14.35	1.88×10^{-6}	6.19
Proposed PABQ ($N_{ibs} = 5 \times 10^5, \epsilon = 10\%$)	$q = 4$ 1 + 1.40 = 2.40	10 + 5.60 = 15.60	1.93×10^{-6}	5.89
	$q = 5$ 1 + 1.35 = 2.35	10 + 6.75 = 16.75	1.91×10^{-6}	8.99
	$q = 2$ 1 + 2.45 = 3.45	10 + 4.90 = 14.90	1.91×10^{-6}	3.74
	$q = 3$ 1 + 1.95 = 2.95	10 + 5.85 = 15.85	1.90×10^{-6}	2.19
Proposed PABQ ($N_{ibs} = 1 \times 10^6, \epsilon = 5\%$)	$q = 4$ 1 + 1.65 = 2.65	10 + 6.60 = 16.60	1.89×10^{-6}	3.70
	$q = 5$ 1 + 1.55 = 2.55	10 + 7.75 = 17.75	1.93×10^{-6}	3.16

Note: AK-MCMC and PABQ are performed 20 independent runs. Thus, for those methods, average results are reported for N_{iter} , N_{call} , and \hat{P}_f . Besides, $\text{COV}[\hat{P}_f]$ is also approximated accordingly.

423 cost of slightly increased N_{iter} and N_{call} .

Table 7: Random variables for Example 4.

Variable	Distribution	Mean	COV
P_0	Lognormal	500 kN	0.20
P_1	Lognormal	200 kN	0.20
P_4	Lognormal	200 kN	0.20
P_7	Lognormal	200 kN	0.20
P_{10}	Lognormal	200 kN	0.20
A	Normal	2000 mm ²	0.15
E	Normal	2.00×10^5 MPa	0.15

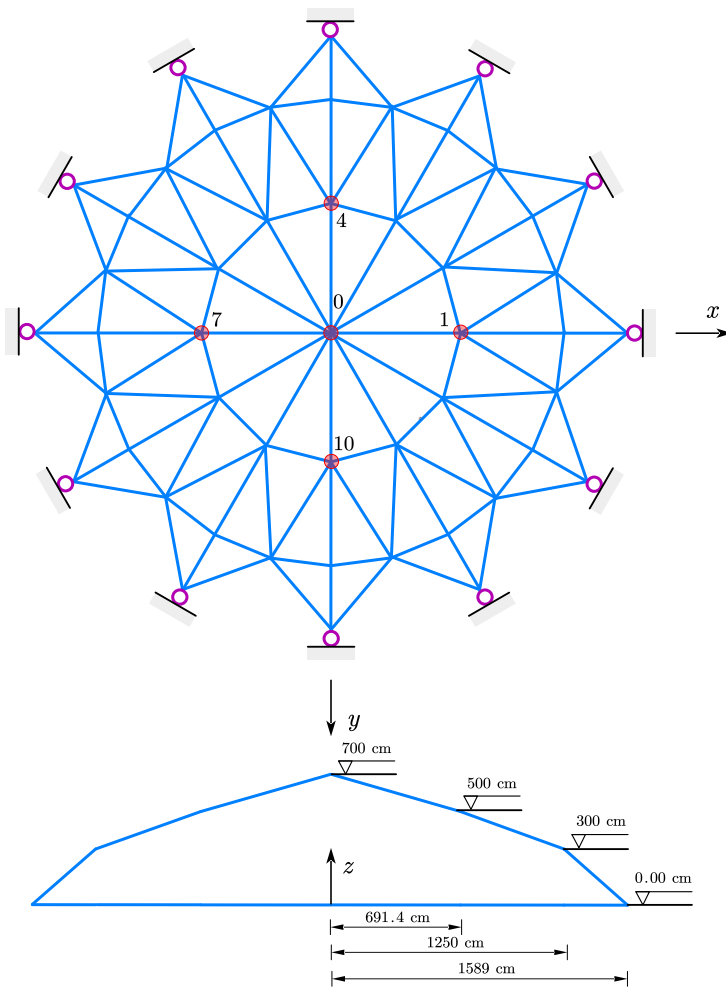


Figure 7: A 120-bar space truss structure.

Table 8: Reliability results for Example 4.

Method	N_{iter}	N_{call}	\hat{P}_f	COV $[\hat{P}_f]$ /%	
MCS	-	10^6	5.08×10^{-4}	4.44	
FORM	7	65	3.16×10^{-4}	-	
SORM	7	172	5.23×10^{-4}	-	
AK-MCS+U	1 + 60.75 = 61.75	12 + 60.75 = 72.75	5.16×10^{-4}	4.84	
ALPI	1 + 47.45 = 48.45	12 + 47.45 = 59.45	5.10×10^{-4}	3.54	
AK-MCMC	-	-	-	-	
Proposed PABQ	$q = 5$	1 + 5.90 = 6.90	10 + 29.50 = 39.50	4.93×10^{-4}	4.74
	$q = 10$	1 + 3.80 = 4.80	10 + 38.00 = 48.00	4.98×10^{-4}	3.31
	$q = 15$	1 + 2.65 = 3.65	10 + 39.75 = 49.75	4.99×10^{-4}	4.68
	$q = 20$	1 + 2.40 = 3.40	10 + 48.00 = 58.00	4.98×10^{-4}	6.22
Proposed PABQ ($N_{ibs} = 1 \times 10^6, \epsilon = 5\%$)	$q = 5$	1 + 8.65 = 9.65	10 + 43.25 = 53.25	5.04×10^{-4}	3.41
	$q = 10$	1 + 4.80 = 5.80	10 + 48.00 = 58.00	5.06×10^{-4}	2.40
	$q = 15$	1 + 3.70 = 4.70	10 + 55.50 = 65.50	5.07×10^{-4}	2.15
	$q = 20$	1 + 2.90 = 3.90	10 + 58.00 = 68.00	5.02×10^{-4}	4.27

Note: For AK-MCS+U and ALPI, the MC population size is set as 10^6 . AK-MCS+U, ALPI and PABQ are performed 20 independent runs. Thus, for those methods, average results are reported for N_{iter} , N_{call} , and \hat{P}_f . Besides, COV $[\hat{P}_f]$ is also approximated accordingly.

424 5. Conclusions

425 This paper presents a ‘Parallel Adaptive Bayesian Quadrature’ (PABQ) method for rare failure event
426 estimation. As it is rooted in ALPI, PABQ offers an alternative framework to the quantification, propagation
427 and reduction of numerical uncertainty for assessing failure probabilities. Besides, compared to ALPI, two
428 important improvements are made in PABQ to enable the use of ever-increasing parallel computing facilities
429 and enhance the capability of assessing small failure probabilities. The parallelism of PABQ is achieved by
430 developing a multi-point selection strategy, while the capableness for rare failure event estimation is realized
431 by proposing an importance ball sampling technique. The performance of the proposed method is illustrated
432 by means of four numerical examples. In most studied cases, it is found that PABQ can not only significantly
433 reduce the average number of iterations (especially when q is large), but also lower the average total number
434 of performance function calls (especially when q is small) compared to several selected existing methods.
435 This indicates the computational efficiency advantage of PABQ in both parallel and non-parallel computing.
436 In addition, PABQ is able to produce accurate estimates for small failure probabilities (e.g., in the order of
437 10^{-7}).

438 The proposed method, in its current form, is not applicable to high-dimensional and/or strongly non-
439 linear problems. The former, on one hand, is due to the challenges of implementing GP models in high
440 dimensions. On the other hand, IBS should not lead to significant improvement for a high-dimensional case.
441 The latter is caused by the fact that the GP model is typically suitable for modelling smooth or moderately
442 nonlinear functions. These drawbacks will be addressed in future work.

443 Declaration of competing interest

444 The authors declare that they have no known competing financial interests or personal relationships that
445 could have appeared to influence the work reported in this paper.

446 Acknowledgments

447 Chao Dang is mainly supported by China Scholarship Council (CSC). Pengfei Wei is grateful to the
448 support from the National Natural Science Foundation of China (grant no. 51905430 and 72171194). Marcos
449 Valdebenito acknowledges the support by ANID (National Agency for Research and Development, Chile)
450 under its program FONDECYT, grant number 1180271. Chao Dang, Pengfei Wei and Michael Beer also
451 would like to appreciate the support of Sino-German Mobility Program under grant number M-0175.

452 Appendix A. Numerical algorithm of the active learning probabilistic integration

453 The procedure for numerical implementation of the ALPI method includes the following steps:
454

455 **Step A.1: Generate a Monte Carlo population**

456 Generate a MC population comprising N_{mc} samples according to $f_{\mathbf{X}}(\mathbf{x})$, denoted by $\overline{\mathcal{X}} = \{\overline{\mathbf{x}}^{(i)}\}_{i=1}^{N_{mc}}$.
 457 This population has two functions: (1) It serves as a candidate sample pool among which the next best
 458 point is identified to evaluate on the g -function; and (2) It is used to evaluate the posterior mean and UPV
 459 of the failure probability (Eqs. (13) and (15)).

460 **Step A.2: Get initial observations**

461 Randomly select N_0 (e.g., 12) samples among $\overline{\mathcal{X}}$, denoted by \mathcal{X} . Those points are then evaluated on
 462 the g -function to get N_0 observations, denoted by \mathcal{Y} . As such, an initial dataset can be constructed, i.e.,
 463 $\mathcal{D} = \{\mathcal{X}, \mathcal{Y}\}$. Let $n = N_0$.

464 **Step A.3: Infer the posterior failure probability**

465 The prior mean and variance functions of $\hat{g}_0 \sim \mathcal{GP}(m_{\hat{g}_0}(\mathbf{x}), k_{\hat{g}_0}(\mathbf{x}, \mathbf{x}'))$ are assumed to be a con-
 466 stant and the squared exponential kernel in this study, respectively. Based on \mathcal{D} , a posterior GP $\hat{g}_n \sim$
 467 $\mathcal{GP}(m_{\hat{g}_n}(\mathbf{x}), k_{\hat{g}_n}(\mathbf{x}, \mathbf{x}'))$ for the g -function can be obtained. This step mainly consists of tuning the hyper-
 468 parameters via maximum likelihood estimation. For convenience, one can use the *fitrgp* function in Statistics
 469 and Machine Learning Toolbox of Matlab. Afterwards, the posterior mean of failure probability can be es-
 470 timated by:

$$\tilde{m}_{\hat{P}_{f,n}} = \frac{1}{N_{mc}} \sum_{i=1}^{N_{mc}} \Phi \left(-\frac{m_{\hat{g}_n}(\overline{\mathbf{x}}^{(i)})}{\sigma_{\hat{g}_n}(\overline{\mathbf{x}}^{(i)})} \right), \quad (\text{A.1})$$

471 and the upper-bound of posterior standard deviation (UPSTD):

$$\tilde{\sigma}_{\hat{P}_{f,n}} = \frac{1}{N_{mc}} \sum_{i=1}^{N_{mc}} \sqrt{\Phi \left(-\frac{m_{\hat{g}_n}(\overline{\mathbf{x}}^{(i)})}{\sigma_{\hat{g}_n}(\overline{\mathbf{x}}^{(i)})} \right) \Phi \left(\frac{m_{\hat{g}_n}(\overline{\mathbf{x}}^{(i)})}{\sigma_{\hat{g}_n}(\overline{\mathbf{x}}^{(i)})} \right)}. \quad (\text{A.2})$$

472 **Step A.4: Check the stopping criterion**

473 Only if the posterior failure probability processes a sufficiently low level of epistemic uncertainty, its
 474 mean can be used to predict the failure probability. To this end, we propose to examine the estimated
 475 upper bound of posterior COV of the failure probability as described next. If $\frac{\tilde{\sigma}_{\hat{P}_{f,n}}}{\tilde{m}_{\hat{P}_{f,n}}} < \epsilon$ is satisfied, go to
 476 **Step A.6**; Else, go to **Step A.5**. Here ϵ is a user-specified threshold, which takes the value of 0.02 in all
 477 numerical examples.

478 **Step A.5: Enrich the previous dataset**

479 At this stage, the best next point to evaluate on the g -function should be identified by a learning function.
 480 By exploring the structure of UPV of failure probability (Eq. (15)), the so-called upper-bound posterior
 481 variance contribution (UPVC) function is introduced [43]:

$$\text{UPVC}(\mathbf{x}) = \sqrt{\Phi \left(-\frac{m_{\hat{g}_n}(\mathbf{x})}{\sigma_{\hat{g}_n}(\mathbf{x})} \right) \Phi \left(\frac{m_{\hat{g}_n}(\mathbf{x})}{\sigma_{\hat{g}_n}(\mathbf{x})} \right)} \times f_{\mathbf{X}}(\mathbf{x}), \quad (\text{A.3})$$

482 where $\bar{\sigma}_{\hat{P}_{f,n}}^2 = [\int_{\mathcal{X}} \text{UPVC}(\mathbf{x})d\mathbf{x}]^2$ holds. The best next point \mathbf{x}^* is selected by:

$$\mathbf{x}^* = \arg \max_{\bar{\mathbf{x}} \in \bar{\mathcal{X}}} \text{UPVC}(\mathbf{x}). \quad (\text{A.4})$$

483 The g -function is then evaluated at the point \mathbf{x}^* , i.e., $y^* = g(\mathbf{x}^*)$. The dataset \mathcal{D} is enriched by $\mathcal{D} =$
484 $\mathcal{D} \cup (\mathbf{x}^*, y^*)$. Let $n = n + 1$, and go to **Step A.3**.

485 **Step A.6: End the algorithm**

486 Return $\tilde{m}_{\hat{P}_{f,n}}$ as the estimated failure probability and end the algorithm.

487 **References**

- 488 [1] S.-K. Au, J. L. Beck, Estimation of small failure probabilities in high dimensions by subset simulation, *Probabilistic*
489 *Engineering Mechanics* 16 (4) (2001) 263–277.
- 490 [2] A. Harbitz, Efficient and accurate probability of failure calculation by the use of importance sampling technique, in:
491 *Proceedings of the 4-th International Conference on Applications of Statistics and Probability in Soil and Structural*
492 *Engineering*, Vol. 4, 1983, pp. 825–836.
- 493 [3] A. Tabandeh, G. Jia, P. Gardoni, A review and assessment of importance sampling methods for reliability analysis,
494 *Structural Safety* 97 (2022) 102216.
- 495 [4] A. M. Hasofer, N. C. Lind, Exact and invariant second-moment code format, *Journal of the Engineering Mechanics Division*
496 *100* (1) (1974) 111–121.
- 497 [5] R. Rackwitz, B. Flessler, Structural reliability under combined random load sequences, *Computers & Structures* 9 (5)
498 (1978) 489–494.
- 499 [6] K. Breitung, Asymptotic approximations for multinormal integrals, *Journal of Engineering Mechanics* 110 (3) (1984)
500 357–366.
- 501 [7] Z. Hu, R. Mansour, M. Olsson, X. Du, Second-order reliability methods: a review and comparative study, *Structural and*
502 *Multidisciplinary Optimization* (2021) 1–31.
- 503 [8] Y. Zhao, Z. Lu, *Structural reliability: approaches from perspectives of statistical moments*, John Wiley & Sons Ltd
504 Chichester, 2021.
- 505 [9] J. Xu, C. Dang, A new bivariate dimension reduction method for efficient structural reliability analysis, *Mechanical*
506 *Systems and Signal Processing* 115 (2019) 281–300.
- 507 [10] T. Zhou, Y. Peng, Adaptive bayesian quadrature based statistical moments estimation for structural reliability analysis,
508 *Reliability Engineering & System Safety* 198 (2020) 106902.
- 509 [11] X. Zhang, M. D. Pandey, Structural reliability analysis based on the concepts of entropy, fractional moment and dimen-
510 sional reduction method, *Structural Safety* 43 (2013) 28–40.
- 511 [12] J. Xu, F. Kong, Adaptive scaled unscented transformation for highly efficient structural reliability analysis by maximum
512 entropy method, *Structural Safety* 76 (2019) 123–134.
- 513 [13] C. Dang, J. Xu, A mixture distribution with fractional moments for efficient seismic reliability analysis of nonlinear
514 structures, *Engineering Structures* 208 (2020) 109912.
- 515 [14] J. Xu, C. Dang, A novel fractional moments-based maximum entropy method for high-dimensional reliability analysis,
516 *Applied Mathematical Modelling* 75 (2019) 749–768.
- 517 [15] C. Dang, J. Xu, Unified reliability assessment for problems with low-to high-dimensional random inputs using the Laplace
518 transform and a mixture distribution, *Reliability Engineering & System Safety* 204 (2020) 107124.

- 519 [16] C. Dang, P. Wei, M. Beer, An approach to evaluation of EVD and small failure probabilities of uncertain nonlinear
520 structures under stochastic seismic excitations, *Mechanical Systems and Signal Processing* 152 (2021) 107468.
- 521 [17] J.-B. Chen, J. Li, Dynamic response and reliability analysis of non-linear stochastic structures, *Probabilistic Engineering*
522 *Mechanics* 20 (1) (2005) 33–44.
- 523 [18] J. Li, J.-B. Chen, Dynamic response and reliability analysis of structures with uncertain parameters, *International Journal*
524 *for Numerical Methods in Engineering* 62 (2) (2005) 289–315.
- 525 [19] J.-B. Chen, J. Li, The extreme value distribution and dynamic reliability analysis of nonlinear structures with uncertain
526 parameters, *Structural Safety* 29 (2) (2007) 77–93.
- 527 [20] J. Li, J.-b. Chen, W.-l. Fan, The equivalent extreme-value event and evaluation of the structural system reliability,
528 *Structural Safety* 29 (2) (2007) 112–131.
- 529 [21] X. Li, G. Chen, H. Cui, D. Yang, Direct probability integral method for static and dynamic reliability analysis of structures
530 with complicated performance functions, *Computer Methods in Applied Mechanics and Engineering* 374 (2021) 113583.
- 531 [22] G. Chen, D. Yang, A unified analysis framework of static and dynamic structural reliabilities based on direct probability
532 integral method, *Mechanical Systems and Signal Processing* 158 (2021) 107783.
- 533 [23] L. Li, G. Chen, M. Fang, D. Yang, Reliability analysis of structures with multimodal distributions based on direct
534 probability integral method, *Reliability Engineering & System Safety* 215 (2021) 107885.
- 535 [24] G. Chen, D. Yang, Y. Liu, H. Guo, System reliability analyses of static and dynamic structures via direct probability
536 integral method, *Computer Methods in Applied Mechanics and Engineering* 388 (2022) 114262.
- 537 [25] C. G. Bucher, U. Bourgund, A fast and efficient response surface approach for structural reliability problems, *Structural*
538 *Safety* 7 (1) (1990) 57–66.
- 539 [26] S.-C. Kang, H.-M. Koh, J. F. Choo, An efficient response surface method using moving least squares approximation for
540 structural reliability analysis, *Probabilistic Engineering Mechanics* 25 (4) (2010) 365–371.
- 541 [27] A. Hadidi, B. F. Azar, A. Rafiee, Efficient response surface method for high-dimensional structural reliability analysis,
542 *Structural Safety* 68 (2017) 15–27.
- 543 [28] C. M. Rocco, J. A. Moreno, Fast monte carlo reliability evaluation using support vector machine, *Reliability Engineering*
544 *& System Safety* 76 (3) (2002) 237–243.
- 545 [29] K. Cheng, Z. Lu, Adaptive bayesian support vector regression model for structural reliability analysis, *Reliability Engi-*
546 *neering & System Safety* 206 (2021) 107286.
- 547 [30] J. Wang, C. Li, G. Xu, Y. Li, A. Kareem, Efficient structural reliability analysis based on adaptive bayesian support vector
548 regression, *Computer Methods in Applied Mechanics and Engineering* 387 (2021) 114172.
- 549 [31] S. Marelli, B. Sudret, An active-learning algorithm that combines sparse polynomial chaos expansions and bootstrap for
550 structural reliability analysis, *Structural Safety* 75 (2018) 67–74.
- 551 [32] B. Bhattacharyya, Structural reliability analysis by a bayesian sparse polynomial chaos expansion, *Structural Safety* 90
552 (2021) 102074.
- 553 [33] I. Kaymaz, Application of kriging method to structural reliability problems, *Structural Safety* 27 (2) (2005) 133–151.
- 554 [34] V. Dubourg, B. Sudret, F. Deheeger, Metamodel-based importance sampling for structural reliability analysis, *Probabilistic*
555 *Engineering Mechanics* 33 (2013) 47–57.
- 556 [35] I. Depina, T. M. H. Le, G. Fenton, G. Eiksund, Reliability analysis with metamodel line sampling, *Structural Safety* 60
557 (2016) 1–15.
- 558 [36] B. J. Bichon, M. S. Eldred, L. P. Swiler, S. Mahadevan, J. M. McFarland, Efficient global reliability analysis for nonlinear
559 implicit performance functions, *AIAA Journal* 46 (10) (2008) 2459–2468.
- 560 [37] B. Echard, N. Gayton, M. Lemaire, AK-MCS: an active learning reliability method combining kriging and monte carlo
561 simulation, *Structural Safety* 33 (2) (2011) 145–154.

- 562 [38] X. Yang, Y. Liu, Y. Gao, Y. Zhang, Z. Gao, An active learning kriging model for hybrid reliability analysis with both
563 random and interval variables, *Structural and Multidisciplinary Optimization* 51 (5) (2015) 1003–1016.
- 564 [39] Z. Lv, Z. Lu, P. Wang, A new learning function for kriging and its applications to solve reliability problems in engineering,
565 *Computers & Mathematics with Applications* 70 (5) (2015) 1182–1197.
- 566 [40] Z. Sun, J. Wang, R. Li, C. Tong, Lif: A new kriging based learning function and its application to structural reliability
567 analysis, *Reliability Engineering & System Safety* 157 (2017) 152–165.
- 568 [41] X. Zhang, L. Wang, J. D. Sørensen, REIF: a novel active-learning function toward adaptive kriging surrogate models for
569 structural reliability analysis, *Reliability Engineering & System Safety* 185 (2019) 440–454.
- 570 [42] Y. Shi, Z. Lu, R. He, Y. Zhou, S. Chen, A novel learning function based on kriging for reliability analysis, *Reliability
571 Engineering & System Safety* 198 (2020) 106857.
- 572 [43] C. Dang, P. Wei, J. Song, M. Beer, Estimation of failure probability function under imprecise probabilities by active
573 learning–augmented probabilistic integration, *ASCE-ASME Journal of Risk and Uncertainty in Engineering Systems,
574 Part A: Civil Engineering* 7 (4) (2021) 04021054.
- 575 [44] B. Echard, N. Gayton, M. Lemaire, N. Relun, A combined importance sampling and kriging reliability method for small
576 failure probabilities with time-demanding numerical models, *Reliability Engineering & System Safety* 111 (2013) 232–240.
- 577 [45] X. Huang, J. Chen, H. Zhu, Assessing small failure probabilities by AK–SS: An active learning method combining kriging
578 and subset simulation, *Structural Safety* 59 (2016) 86–95.
- 579 [46] P. Wei, C. Tang, Y. Yang, Structural reliability and reliability sensitivity analysis of extremely rare failure events by
580 combining sampling and surrogate model methods, *Proceedings of the Institution of Mechanical Engineers, Part O:
581 Journal of Risk and Reliability* 233 (6) (2019) 943–957.
- 582 [47] T. Zhou, Y. Peng, Structural reliability analysis via dimension reduction, adaptive sampling, and monte carlo simulation,
583 *Structural and Multidisciplinary Optimization* 62 (5) (2020) 2629–2651.
- 584 [48] T. Zhou, Y. Peng, Active learning and active subspace enhancement for pdem-based high-dimensional reliability analysis,
585 *Structural Safety* 88 (2021) 102026.
- 586 [49] Y. Liu, L. Li, S. Zhao, S. Song, A global surrogate model technique based on principal component analysis and kriging
587 for uncertainty propagation of dynamic systems, *Reliability Engineering & System Safety* 207 (2021) 107365.
- 588 [50] Y. Peng, T. Zhou, J. Li, Surrogate modeling immersed probability density evolution method for structural reliability
589 analysis in high dimensions, *Mechanical Systems and Signal Processing* 152 (2021) 107366.
- 590 [51] T. Zhou, Y. Peng, Kernel principal component analysis-based gaussian process regression modelling for high-dimensional
591 reliability analysis, *Computers & Structures* 241 (2020) 106358.
- 592 [52] M. M. Zuniga, A. Murangira, T. Perdrizet, Structural reliability assessment through surrogate based importance sampling
593 with dimension reduction, *Reliability Engineering & System Safety* 207 (2021) 107289.
- 594 [53] J. Yin, X. Du, Active learning with generalized sliced inverse regression for high-dimensional reliability analysis, *Structural
595 Safety* 94 (2022) 102151.
- 596 [54] R. Teixeira, M. Nogal, A. O’Connor, B. Martinez-Pastor, Reliability assessment with density scanned adaptive kriging,
597 *Reliability Engineering & System Safety* 199 (2020) 106908.
- 598 [55] R. Li, X. Liang, Q. Peng, A selection strategy for kriging based design of experiments by spectral clustering and learning
599 function, *ASCE-ASME Journal of Risk and Uncertainty in Engineering Systems, Part B: Mechanical Engineering* 7 (2)
600 (2021) 020902.
- 601 [56] Z. Chen, G. Li, J. He, Z. Yang, J. Wang, A new parallel adaptive structural reliability analysis method based on importance
602 sampling and k-medoids clustering, *Reliability Engineering & System Safety* 218 (2022) 108124.
- 603 [57] R. Teixeira, M. Nogal, A. O’Connor, Adaptive approaches in metamodel-based reliability analysis: A review, *Structural
604 Safety* 89 (2021) 102019.

- 605 [58] A. O'Hagan, Bayes-hermite quadrature, *Journal of Statistical Planning and Inference* 29 (3) (1991) 245–260.
- 606 [59] C. E. Rasmussen, Z. Ghahramani, Bayesian monte carlo, *Advances in Neural Information Pprocessing Systems* (2003)
607 505–512.
- 608 [60] P. Wei, X. Zhang, M. Beer, Adaptive experiment design for probabilistic integration, *Computer Methods in Applied
609 Mechanics and Engineering* 365 (2020) 113035.
- 610 [61] V. Lalchand, C. E. Rasmussen, Approximate inference for fully bayesian gaussian process regression, in: *Symposium on
611 Advances in Approximate Bayesian Inference*, PMLR, 2020, pp. 1–12.
- 612 [62] A. R. Voelker, J. Gosmann, T. C. Stewart, Efficiently sampling vectors and coordinates from the n-sphere and n-ball,
613 *Centre for Theoretical Neuroscience-Technical Report* (2017).
- 614 [63] J. Li, J. Chen, *Stochastic dynamics of structures*, John Wiley & Sons, 2009.
- 615 [64] D. J. MacKay, D. J. Mac Kay, *Information theory, inference and learning algorithms*, Cambridge university press, 2003.
- 616 [65] S. Marelli, R. Schöbi, B. Sudret, UQLab user manual – Structural reliability (Rare event estimation), Tech. rep., Chair of
617 Risk, Safety and Uncertainty Quantification, ETH Zurich, Switzerland, report UQLab-V2.0-107 (2022).
- 618 [66] R. Schöbi, B. Sudret, S. Marelli, Rare event estimation using polynomial-chaos kriging, *ASCE-ASME Journal of Risk and
619 Uncertainty in Engineering Systems, Part A: Civil Engineering* 3 (2) (2017) D4016002.
- 620 [67] A. Borri, E. Speranzini, Structural reliability analysis using a standard deterministic finite element code, *Structural Safety*
621 19 (4) (1997) 361–382.
- 622 [68] I. Papaioannou, S. Geyer, D. Straub, Improved cross entropy-based importance sampling with a flexible mixture model,
623 *Reliability Engineering & System Safety* 191 (2019) 106564.